The organizational principles of de-differentiated topographic maps

Peng Liu[1,2,6], Anastasia Chrysidou[1,2,6], Juliane Doehler[1,2], Thomas Wolbers[2,3,6], Esther Kuehn[1,2,3,6*]

[1] Institute for Cognitive Neurology and Dementia Research (IKND), Otto-von-Guericke University Magdeburg, 39120, Germany

[2] German Center for Neurodegenerative Diseases (DZNE), Magdeburg, 30120, Germany

[3] Center for Behavioral Brain Sciences (CBBS) Magdeburg, Magdeburg, 39120, Germany

[6] these authors contributed equally

Corresponding author & Lead contact:

Esther Kuehn, PhD

Institute for Cognitive Neurology and Dementia Research (IKND), Otto-von-Guericke University Magdeburg, 39120, Germany

Email: esther.kuehn@dzne.de

Abstract

Topographic maps are a fundamental feature of cortex architecture in the mammalian brain. One common theory is that the de-differentiation of topographic maps links to impairments in everyday behavior due to less precise functional map readouts. Here, we tested this theory by characterizing de-differentiated topographic maps in primary somatosensory cortex (SI) of younger and older adults by means of ultra-high resolution functional magnetic resonance imaging together with perceptual finger individuation and hand dexterity. Older adults' SI maps showed similar amplitude, size, and levels of stimulus-related noise than younger adults' SI maps, but presented with less representational similarity between distant fingers. Larger population receptive field sizes in older adults' maps did not correlate with behavior, whereas reduced cortical distances related to better hand dexterity. Our data uncover the drawbacks of a simple de-differentiation model of topographic map function, and motivate the introduction of a feature-based model of cortical reorganization.

Keywords

adaptive, aging, cortex, neurodegeneration, plasticity, 7 Tesla MRI, meso-scale, somatosensation, somatotopy, touch

Introduction

Topographic maps are a fundamental feature of cortex architecture and can be found in all sensory systems and in many motor systems of the mammalian brain. Topographic units organize subcortical brain structures such as the thalamus, the globus pallidus, and the striatum (Crabtree, 1992; Hintiryan et al., 2016; Zeharia et al., 2015), primary sensory input and output areas such as primary sensory and motor cortices (Penfield and Boldrey, 1937), and higher-level integrative brain areas such as the medial and superior parietal cortices and the cingulate cortex (Sereno and Huang, 2006; Zeharia et al., 2019, 2015). Topographic maps and their malfunctions give rise to a multitude of sensory, motor, and cognitive functions and associated deficits (Amedi et al., 2003; Kalisch et al., 2009; Kikkert et al., 2019; Kuehn et al., 2018; Makin et al., 2013a; Saadon-Grosman et al., 2015), which warrants a precise understanding of their organizational features.

One common theory posits that the 'de-differentiation' of topographic maps represents one mechanism of their malfunction. Cortical de-differentiation can be conceptualized as greater map activation (Pleger et al., 2016), a larger topographic map area (Kalisch et al., 2009), but also more noisy topographic units and/or less cortical inhibition between neighbouring topographic units (Lenz et al., 2012; Pleger et al., 2016). Such changes are particularly observed in older adults' topographic maps, and one common model on cortical aging assumes 'overactivated' or more 'de-differentiated' topographic maps in older compared to younger adults, which are assumed to explain reduced sensory, motor, and cognitive abilities of older adults in everyday life (Cabeza, 2002; Cassady et al., 2020; Dennis and Cabeza, 2011; Heuninckx et al., 2008; Mattay et al., 2002; Reuter-Lorenz and Lustig, 2005; Riecker et al., 2006). However, the precise topographic features that characterize a presumably

'de-differentiated' map are so far not clarified, neither are the precise behavioral phenotypes that relate to different aspects of topographic map change.

Here, we used the hand area of the primary somatosensory cortex (SI) in younger and older adults as a model system to study the precise meso-scale features that characterize the presumably de-differentiated topographic maps of older adults, and their relation to behavior. Topographic maps in SI are a suitable model system to investigate basic aspects of cortical de-differentiation, because the tactile modality is not artificially corrected by glasses or hearing aids, and therefore offers access to the 'pure' architecture of the (altered) system. We assessed the functional architecture of topographic maps subject-wise at fine-grained detail using ultra-high field functional magnetic resonance imaging (7T-fMRI), and investigated sensory readouts as well as everyday hand movement capabilities of our participants. 7T-fMRI is a valuable method for describing fine-grained features of topographic maps, because it allows mapping small-scale topographic units, such as individual fingers, subject-wise and with high levels of accuracy and reproducibility (Kolasinski et al., 2016a; Kuehn et al., 2018; Kuehn and Sereno, 2018; O'Neill et al., 2020). Recently, this allowed the precise description of features that characterize non-afferent maps in human SI (Kuehn et al., 2018), SI map changes after short-term plasticity (Kolasinski et al., 2016b), or movement-dependent maps in motor cortex (Huber et al., 2020).

To systematically characterize the meso-scale features of de-differentiated topographic maps and their relation to behavior, we distinguished between global changes of the map that were present across all topographic units (here fingers), and local changes of the map that only covered parts of the map. This distinction is relevant due to the nonhomogeneous use of individual fingers in everyday life (Belić and Faisal, 2015), the non-uniform microstimulation-evoked muscle activity in motor cortex (Overduin et al., 2012), and for differentiating between age-dependent and use-dependent plasticity (Makin et al., 2013a). We also distinguished between topographic map features that link to functional separation, as here tested by perceptual finger individuation, and those that require functional integration, as here tested by perceptual finger confusion and motor movements (see **Fig. 1**). A cohort of healthy younger (21-29 years) and healthy older (65-78 years) adults was invited to several experimental sessions, where touch to their fingertips was applied in the 7T-MR scanner using an automated Piezo-driven tactile stimulator (Miller et al., 2018; Schmidt and Blankenburg, 2018). They were also tested behaviorally in a finger mislocalization task (Schweizer et al., 2000) and in different aspects of hand dexterity (Kalisch et al., 2008). By combining ultra-high resolution functional imaging with population receptive field mapping, Fourier-based functional analyses, psychophysics and measures of everyday behavior, we could compare precise map features between younger and older adults' topographic maps, and link these to behavioral phenotypes relevant for everyday life. We could therefore test the basic assumption that de-differentiated cortical maps relate to impairments in everyday behavior. By targeting a mechanism that is assumed to be a hallmark feature of cortical aging, our data also help to uncover a fundamental principle of brain aging.

Results

Topographic maps do not differ in size, amplitude and variability between age groups

We used 7T-fMRI data to compare the fine-grained architecture of topographic finger maps in SI between younger and older adults. Older adults were expected to present with more 'de-differentiated' cortical maps compared to younger adults, which is assumed to link to higher map amplitude and larger map size (Kalisch et al., 2009; Pleger et al., 2016). While undergoing MRI scanning, younger and older adults were stimulated at the fingertips of their right hand using an automated Piezo-driven stimulation system, and different stimulation protocols (see **Fig. 1**). Participants were stimulated at each finger at their 2.5-fold individual threshold to exclude topographic map changes that were due to peripheral (nerve or skin) differences between younger and older adults. We focused on topographic maps in area 3b of SI, because this area is the likely human homologue of the monkey SI cortex (Kaas, 2012).

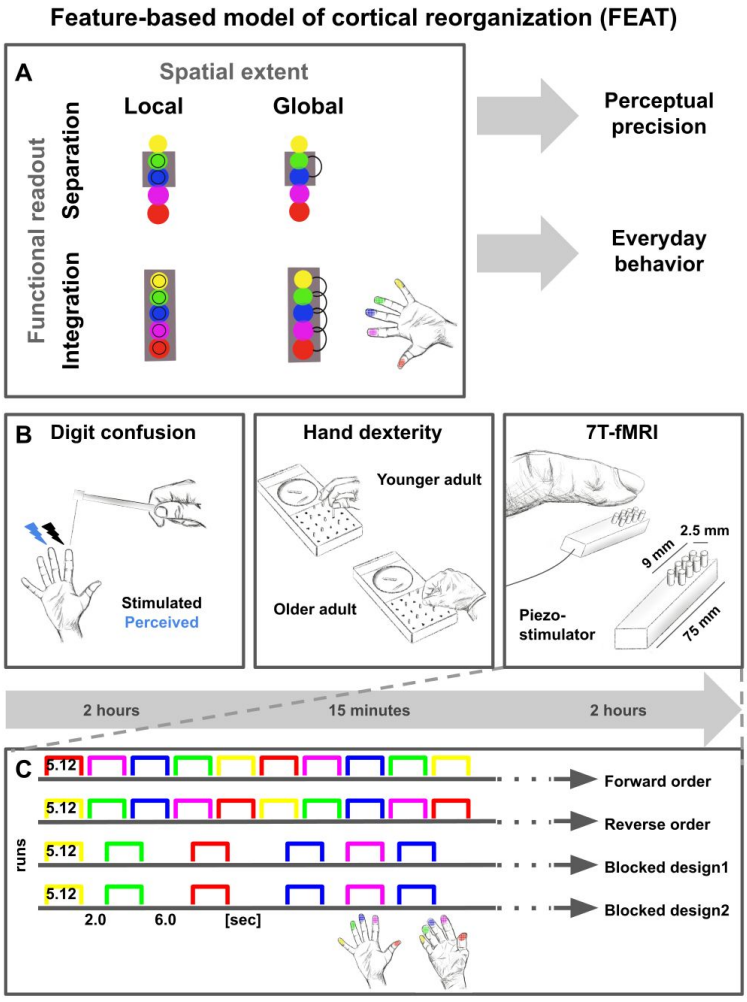

Figure 1. Feature-based characterization of topographic maps using 7T-fMRI and behavioral tests. **A**: FEATure-based map classification allowed us to separate local from global map changes, and differences in integration from differences in separation. **B**: Younger and older adults were tested in a behavioral digit confusion task at their perceptual thresholds (see **Supplemental Figure 1** for tactile detection thresholds) where their ability to locate threshold-touch to the correct finger was investigated (*left*). They were also characterized for individual differences in hand dexterity using the Purdue Pegboard Test, the Grooved Pegboard Test, and the O'Connor Dexterity Test (*middle*). Participants underwent 7T-fMRI at a separate testing day, where tactile finger stimulation was applied using an automated Piezo stimulator (*right*). **C**: In the 7T-MRI scanner, different stimulation protocols were tested in separate runs (each row represents one run).

Significant topographic finger maps in contralateral area 3b in response to finger stimulation were detected in younger and older adults, and across the group as a significant group effect

(see **Fig. 2A-C**). The expected topographic alignment of the fingers (thumb [D1], index finger [D2], middle finger [D3], ring finger [D4], and small finger [D5] arranged superior -> inferior in area 3b) was visible in all individuals of both age groups (see **Fig. 2C**). The mean surface area that topographic maps covered in area 3b, % signal change within the map area, and mean f-values did not differ significantly between age groups (original surface area: $t(34)=0.04$, $p=.97$, resampled surface area; $t(34)=-0.15$, $p=.88$; % signal change: $t(34)=1.17$, $p=.25$; f-value: $t(34)=0.84$, $p=.41$, see **Fig. 2D-G**).

One further variable that may explain age-related differences in topographic maps is the variability of topographic map alignments *within* age groups that may be due to increased internal noise. One may expect the variability to be higher in older adults compared to younger adults topographic maps (McGregor et al., 2012). To inspect topographic map variability within each age group, we calculated the dispersion index *d*, which indicates map stability across the group (*d*=1 indicates perfectly aligned vectors independent of vector amplitude, whereas lower *d* indicates less stable topographic arrangements between individuals in one group). Younger participants showed slightly lower *d* in the topographic map area compared to older adults (*d* young: 0.68, *d* old: 0.72). The variability of topographic map alignments within each age group was therefore generally low, and slightly *higher* in younger compared to older adults (see **Fig. 2B**).

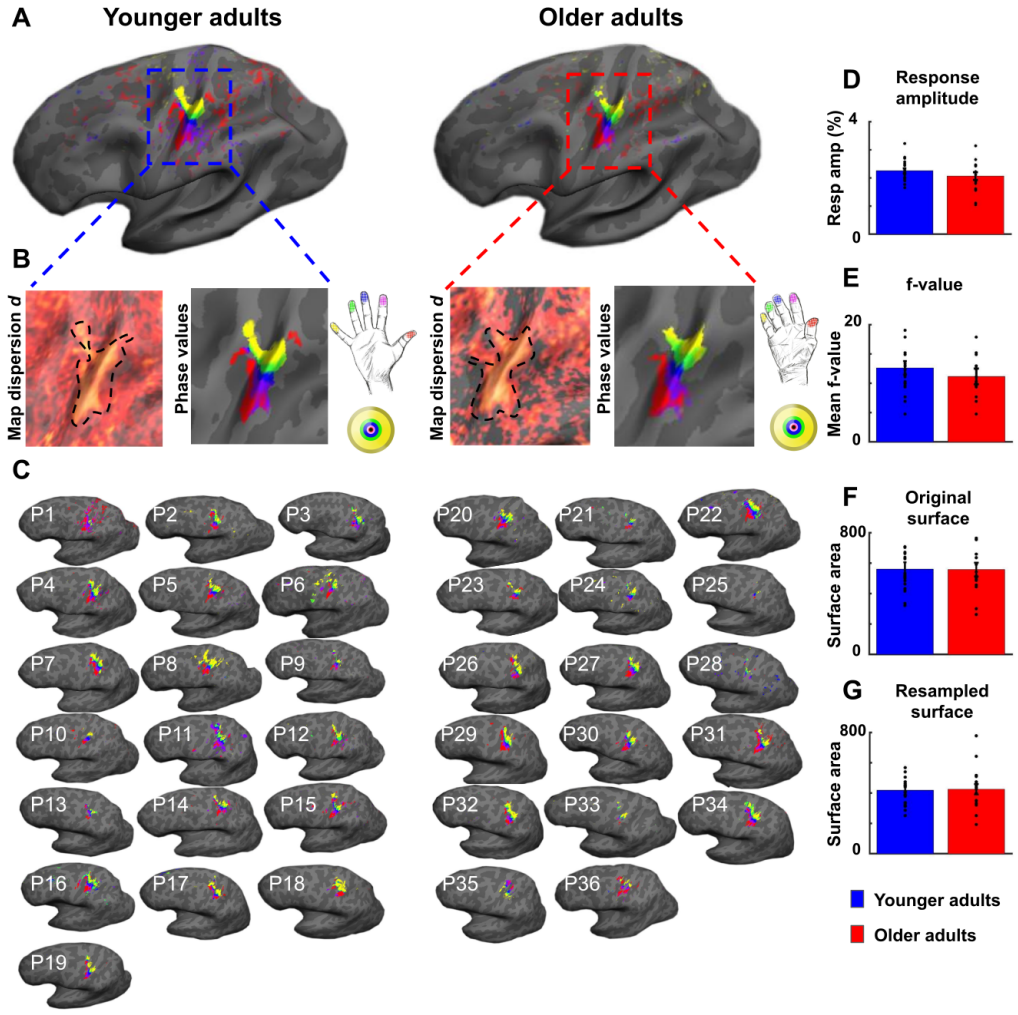

Figure 2. Topographic maps do not differ in size, amplitude and variability between age groups. **A**: Significant topographic finger maps of younger and older adults averaged over the group. Data are visualized on average surfaces of the current set of subjects (younger/older). **B**: Map dispersion *d* and Fourier transformed data of significant topographic group maps of younger and older adults. Lower *d* indicates less stable topographic arrangements over the group. Dotted lines indicate the area of the significant topographic map. **C**: Significant topographic maps of each single participant (P1-P36). **D**: Response amplitudes (in %) of topographic maps compared between younger and older adults (mean +/- SE and individual data). **E**: f-values of topographic maps compared between younger and older adults (mean +/- SE and individual data). **F&G**: Surface area of topographic maps of younger and older adults; values extracted from original (**F**) and resampled (**G**) surfaces (mean +/- SE and individual data). Shown are data of n=19 younger adults and n=17 older adults.

Reduced cortical distances between D2 and D3 in older adults

Previous studies found *larger* cortical distances between D2 and D5 in older compared to younger adults, which was argued to evidence an enlargement of topographic maps in older

adults (Kalisch et al., 2009). We used both absolute (Euclidean) and surface-based (geodesic) cortical distance measures to compare distances of digit representations between younger and older adults (see **Fig. 3C**). An ANOVA with the factors finger-pair and age calculated on Euclidean distances revealed a significant main effect of finger-pair ($F(3,102)=11.20$, $p<10^{-5}$), no main effect of age ($p>.2$), but a significant interaction between finger-pair and age ($F(3)=3.23$, $p<.05$). The main effect of finger-pair was due to increased Euclidean distances between D1 and D2 compared to D3 and D4 ($t(35)=5.57$, $p<.00001$), reduced Euclidean distances between D1 and D2 compared to D4 and D5 ($t(35)=4.87$, $p<.0001$), increased Euclidean distances between D2 and D3 compared to D3 and D4 ($t(35)=3.24$, $p<.01$), and reduced Euclidean distances between D2 and D3 compared to D4 and D5 ($t(25)=2.93$, $p<.01$) across age groups (see **Fig. 3A**). The interaction between finger-pair and age was driven by significantly *reduced* Euclidean distances between D2 and D3 in older adults compared to younger adults (Euclidean distance D2-D3 young: 7.67±0.80, D2-D3 old: 4.98 ± 0.40, $p<.05$, see **Fig. 3A, E**). The latter effect was replicated for geodesic distances, where older adults showed significantly reduced geodesic distances compared to younger adults only between D2 and D3 (Geodesic distance D2-D3 young: 7.80 mm±0.72 mm, old: 5.72 mm±0.64 mm, $p<.05$, see **Fig. 3B**). Effect size analyses using bootstrapping confirm large Hedge's g for Euclidean and geodesic distances between D2 and D3, and low Hedge's g for all other distances (D2-D3 Euclidean: $g=.73$, LCI=.12, UCI=1.45; D2-D3 Geodesic: $g=.69$, LCI=.08, UCI=1.45, all other distances $g<.3$, see **Fig. 3D**). There was no significant correlation between cortical distance between D2 and D3 and individual age, neither for Euclidean nor for geodesic distances (see **Supplemental Figure 2**).

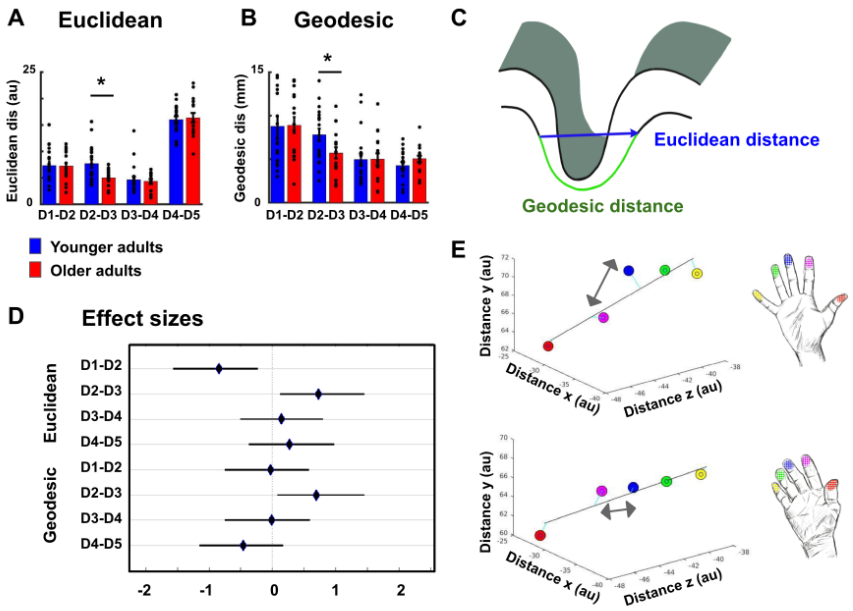

Figure 3. Reduced cortical distances between D2 and D3 in older adults. **A**, **B**: Cortical distances between digit representations in younger and older adults estimated as total (Euclidean) distance (**A**) and as surface-based (geodesic) distance (**B**) (mean ± SEM and individual data) **C**: Schematic visualization of cortical distance measures. **D**: Effect sizes (Hedge's g and 95% confidence intervals) for Euclidean and geodesic distances. **E**: Spatial alignment of younger adults' (*top*) and older adults (*bottom*) digit representations in area 3b. Line represents linear fit, arrows highlight significant differences in cortical distance between younger and older adults. Shown are data of n=19 younger adults and n=17 older adults.

Larger population receptive field (pRF) sizes in older adults

Previous studies on rats had indicated larger receptive field sizes in the hindpaw but not forepaw representation of older compared to younger rats (Godde et al., 2002). This left open the question whether or not there are enlarged population receptive field (pRF) sizes in the human hand area in older compared to younger humans. Bayesian pRF modeling was employed to model pRFs in individual topographic maps, and to compare pRF sizes between younger and older adults (Puckett et al., 2020). pRF distances were used to individuate the five fingers, and pRF sizes were extracted map- and finger-specific in each individual (Puckett et al., 2020) (see **Fig. 4C**). pRF distances revealed an organized finger map with D1-D5 arranged from superior to inferior, as expected (see **Fig. 4A**). An ANOVA with the factors age and finger calculated on pRF sizes showed a significant main effect of finger ($F(4)=7.86$, $p<.0001$), a significant main effect of age ($F(1)=5.00$, $p<.05$), but no significant interaction between age and finger ($F(4)=0.62$, $p>.6$). The main effect of finger was due to significantly larger pRF sizes of D1 compared to D2 (D1: 4.26±0.85, D2: 5.69±1.77, $t(66)=-4.30$, $p<.00006$), D1 compared to D4 (D4: 7.11±2.99, $t(69)=-5.40$, $p<10^{-5}$), D1 compared to D5 (D5: 6.23±3.21, $t(66)=-3.52$, $p<.0008$), D2 compared to D3 (D3: 4.66±2.23, $t(62)=2.05$, $p<.05$), D2 compared to D4 ($t(61)=-2.31$, $p<.02$), D3 compared to D4 ($t(59)=-3.62$, $p<.0006$) and D3 compared to D5 ($t(62)=2.26$, $p<.03$). The main effect of age was due to larger pRF sizes in older compared to younger adults (see **Fig. 4C**).

Because greater pRF sizes may be associated with greater cortical overlap between neighbouring finger representations, dice coefficients were used to compare the overlap of neighbouring digit representations between younger and older adults. When computing an ANOVA with the factors finger-pair and age, there was a trend towards a significant main effect of age ($F(1,31)=3.83$, $p=.059$), and there was a significant effect of finger-pair ($F(3, 93)=7.29$, $p<10^{-3}$). The trend towards the significant effect of age was due to higher mean dice coefficients in older adults compared to younger adults (dice coefficient older: 0.19±0.02, younger: 0.13±0.01, see **Fig. 4B**). Correlation analysis between mean pRF sizes across fingers and mean dice coefficients across fingers did not reveal a significant relationship (see **Fig. 4D** for statistics). Correlation analysis between mean pRF sizes across fingers (for younger and older adults, respectively) and mean cortical distances (i.e., total (Euclidean) distance and surface-based (geodesic) distance, respectively) also did not disclose significant relationships (see **Supplemental Figure 3**). Correlations between average pRF sizes and behavioural measures (i.e., finger individuation and hand dexterity) did not reveal significant relationships (see **Supplemental Figure 3**).

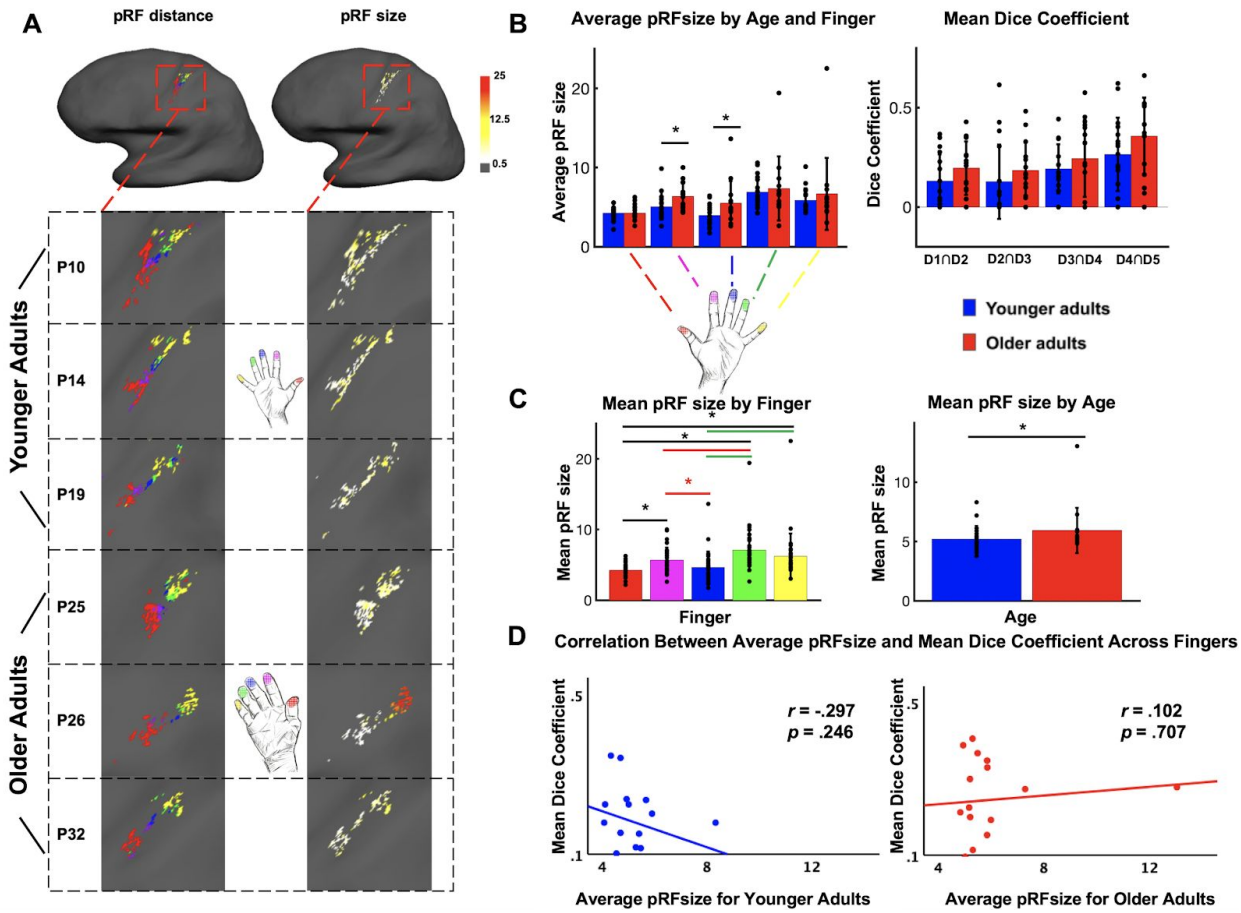

Figure 4. **Larger population receptive field (pRF) sizes in older adults compared to younger adults.** **A:** pRF distances (which encode each individual finger, *left*) and pRF sizes (which encode the size of each finger representation, *right*) shown for six individual participants (randomly chosen, participant numbers same as in **Figure 2**). **B:** pRF sizes per finger and dice coefficients for younger and older adults (mean ± SEM and individual data). **C:** Visualization of significant main effect of finger (*left*) and significant main effect of age (*right*) of pRF sizes (mean ± SEM and individual data). **D**: Correlation between average pRF sizes and mean dice coefficients across fingers for younger and older adults. Correlations between average pRF sizes and cortical distances, and between average pRF sizes and behavioural measures are shown in **Supplemental Figure 3**. Shown are data of n=19 younger adults and n=17 older adults (**A**, **B**, **C**) and of n=17 younger adults and n=16 older adults (**D**).

Lower representational similarity between distant digits in older adults

Another aspect of cortical de-differentiation is the assumed increased 'blurriness' of de-differentiated cortical maps. This was investigated here by using representational similarity analyses, and resting state signal correlations. We used across-run representational similarity analyses to compare the similarity of digit representations between different runs within area 3b (Kuehn et al., 2018). We computed an ANOVA with the factors neighbour and age on finger-specific representational similarity, which revealed a significant effect of neighbour ($F(4,136)=128.6$, $p<10^{-44}$), no main effect of age, but a significant interaction between age and neighbour ($F(4)=3.63$, $p<.05$). The main effect of neighbour was due to higher representational

similarity between 1st neighbour fingers (N1) compared to 2nd, 3rd and 4th neighbour fingers (N2-N4) across age groups. This was expected, because finger stimulation is expected to excite neighbouring fingers more than distant fingers. Critically, the interaction between age and neighbour was due to *lower* representational similarity in older compared to younger adults' SI maps for N3 (N3-similarity young: 0.01±0.03, old: -0.11±0.04, $p<.05$, see **Fig. 5B**). N3 representational similarity correlated negatively with age in older but not in younger adults (see **Supplemental Figure 2** for complete statistics).

To test for local (finger-specific) differences, an ANOVA with the factors digit-pair and age was calculated, which revealed a significant main effect of digit-pair ($F(3,102)=2.88$, $p<.05$), but no main effect of age, and no interaction between age and digt-pair. The significant effect of digit-pair was due to lower representational similarity between D2 and D3 compared to D4 and D5 ($t(35)=2.18$, $p<.05$), and lower representational similarity between D3 and D4 compared to D4 and D5 ($t(35)=2.96$, $p<.05$) across age groups.

Resting state data were used to investigate whether the observed age-related differences in representational similarity between N3-fingers were also reflected in differences in slow frequency fluctuations during rest (Kuehn et al., 2017). Cross-correlation analyses revealed the highest correlations between time series using zero-lag correlations (tested were all possible lags between -130 to +130 TRs). This was true for all possible finger combinations. An ANOVA with the factors neighbour and age on zero-lag cross-correlation coefficients revealed no main effect of neighbour ($F(4,88)=1.50$, $p=.21$), a trend towards a significant main effect of age ($F(1,22)=2.77$, $p=.11$), but no interaction between age and neighbour ($F(4)=0.73$, $p=.57$). An ANOVA with the factors finger and age revealed no main effect of finger ($F(4,88)=0.66$, $p=.62$), a trend towards a significant main effect of age ($F(1,22)=2.43$, $p=.13$), but no interaction between age and finger ($F(4)=0.46$, $p=.76$). The trend for the main effect of age was due to older adults showing higher correlation coefficients across neighbours and fingers compared to younger adults (see **Fig. 5C,D**).

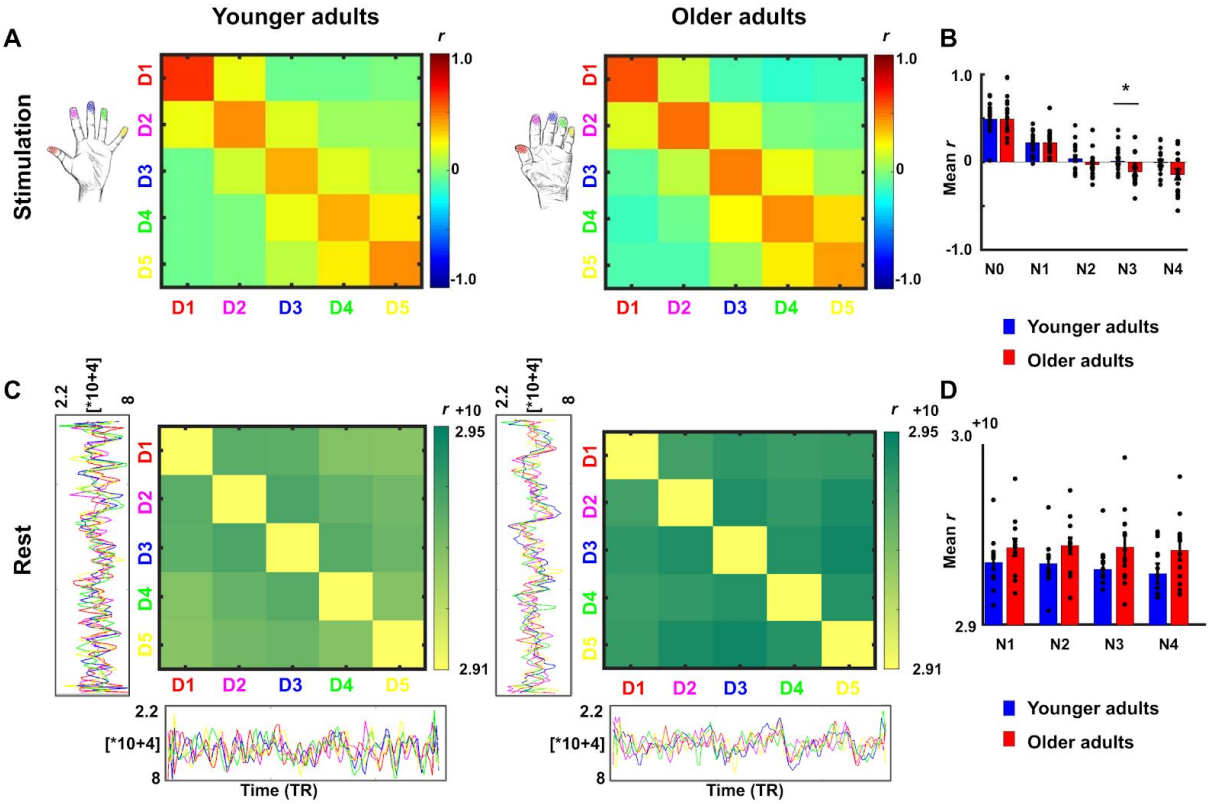

Figure 5. **Lower representational similarity between distant digits in older adults**. **A**: Between-run representational similarity matrices of finger representations in younger and older adults. Higher values indicate higher representational similarity in area 3b. **B**: Mean representational similarity between same fingers (N0), 1st neighbour fingers (N1), 2nd neighbour fingers (N2), 3rd neighbour fingers (N3), and 4th neighbour fingers (N4) (mean +/- SE and individual data). For correlations between N3 representational similarity with individual age see **Supplemental Figure 2**. **C**: Cross-correlations between finger-specific time series of resting state data. On the x- and y-axes, exemplary finger-specific time series for one younger adult and one older adult are shown. TR = Repetition time, where each TR represents one volume. Note that the diagonal shows autocorrelations between resting state time series. **D**: Mean cross-correlation coefficients of resting state data between N1-N4 in younger and older adults (mean +/- SE and individual data). Shown are data of n=19 younger adults and n=17 older adults (**A**,**B**) and data of n=12 younger adults and n=12 older adults (**C**,**D**).

Mislocalizations reflect representational similarity of topographic fields

We used a behavioral finger mislocalization task to test whether the above described functional markers of cortical de-differentiation in area 3b have perceptual correlates. For this purpose, we used a perceptual task that is expected to reflect individual differences in topographic map architecture (Schweizer et al., 2001, 2000). During the task, participants were touched at the fingertips of their right hand at their individual 50%-threshold (see **Fig. 1** for graphical overview, see **Supplemental Figure 1** for individual tactile detection thresholds), and were asked to name the location of finger touch in a five-choice-forced-response paradigm (possible answers were ‘thumb’, ‘index finger’, ‘middle finger’, ‘ring finger’, or ‘small finger’). Mislocalizations (i.e., errors

where participants assigned touch to another finger than the one that was stimulated) are the variable of interest in this task, because mislocalizations are assumed to be driven by overlapping and/or more similar representations in SI that cause perceptual confusion (Pilz et al., 2004). In total, the applied stimulation resulted in 41.10% of mislocalizations across all fingers and groups, which was expected due to the 50%-threshold that was applied during stimulation.

We first tested whether the distribution of mislocalizations followed the expected pattern of *higher than chance* mislocalizations to *adjacent* fingers and *lower than chance* mislocalizations to *distant* fingers. This pattern is expected if the task reflects the adjacency of cortical representations (Schweizer et al., 2000). For younger adults, more mislocalizations than expected by chance were detected at N1, N2, and N3, whereas less mislocalizations than expected by chance were detected at N4. For older adults, more mislocalizations than expected by chance were detected at N1 and N2, and less mislocalizations than expected by chance at N3 and N4 (see **Fig. 6C** and **Supplemental Figure 4**). The comparison of the measured distribution of mislocalization with the proportional distribution as expected by chance showed a significant difference for both age groups (younger adults: $G(3)=9.33$, $p<.05$; older adults: $G(3)=43.59$, $p<.001$). There was a trend towards older adults showing in total more mislocalizations compared to younger adults (older: M=0.45 ± 0.03, younger: M=0.38 ± 0.03, $t(48)=1.69$, $p=.097$, see **Supplemental Figure 4**).

We tested whether the above identified age-related difference in functional map architecture (i.e., less representational similarity between N3-fingers) present with a perceptual correlate. For this aim, we computed an ANOVA with the factors neighbour and age on relative mislocalizations (in %). There was a main effect of neighbour ($F(2.26,108.34)=108.30$, $p<.001$), no significant main effect of age ($p=1$), and a trend towards a significant interaction between neighbour and age ($F(2.26,108.34)=2.50$, $p=.08$). The main effect of neighbour was due to significantly more mislocalizations to N1 compared to N2 ($t(83.54)=5.82$, $p<.001$), to N1 compared to N3 ($t(98)=11.64$, $p<.001$), to N1 compared to N4 ($t(79.97)=17.54$, $p<.001$), to N2 compared to N3 ($t(98)=7.66$, $p<.001$), to N2 compared to N4 ($t(98)=15.40$, $p<.001$), and to N3 compared to N4 ($t(98)=7.03$, $p<.001$) across age groups. This is expected based on the higher amount of mislocalizations to nearby compared to distant fingers, as outlined above. The trend towards a significant interaction between neighbour and age was due to older participants showing less mislocalizations to N3 compared to younger participants (older: 0.15±0.01, younger: 0.21±0.02, $t(48)=-2.52$, $p<.05$, see **Fig. 6D**). Less representational similarity between N3-fingers in older adults as identified using 7T-fMRI was therefore accompanied with less perceptual digit confusion between N3-fingers as tested behaviorally in the same participants, but on a separate testing day.

Mislocalizations reflect adjacency of cortical representations

We then tested whether the above identified age-related differences in finger-specific map architecture (i.e., less cortical distance between D2 and D3) present with a perceptual correlate.

For this aim, we computed one robust ANOVA with the factors digit and age for each of the five stimulated fingers on the relative distribution of mislocalizations (in %). We found a main effect of digit, which was due to more mislocalizations to the respective neighbouring digit/s, as outlined above (see **Supplemental Figure 5** for complete statistics). Importantly, we also found a significant interaction between age and digit for D2 ($F(3,22.02)=4.84$, $p<.05$). *Post hoc* tests revealed that older adults showed higher percentages of mislocalizations from D2 to D3 compared to younger adults (older: M=41.09±5.75, younger: M=17.56±4.19, $t(27.73)=3.96$, $p<.001$, see **Fig. 6E,** see **Supplemental Figure 5** for complete statistics). Reduced cortical distances between the representations of D2 and D3 in older adults, as identified using 7T-fMRI, was therefore accompanied with more perceptual confusion between D2 and D3 as tested behaviorally in the same participants, but on a separate testing day.

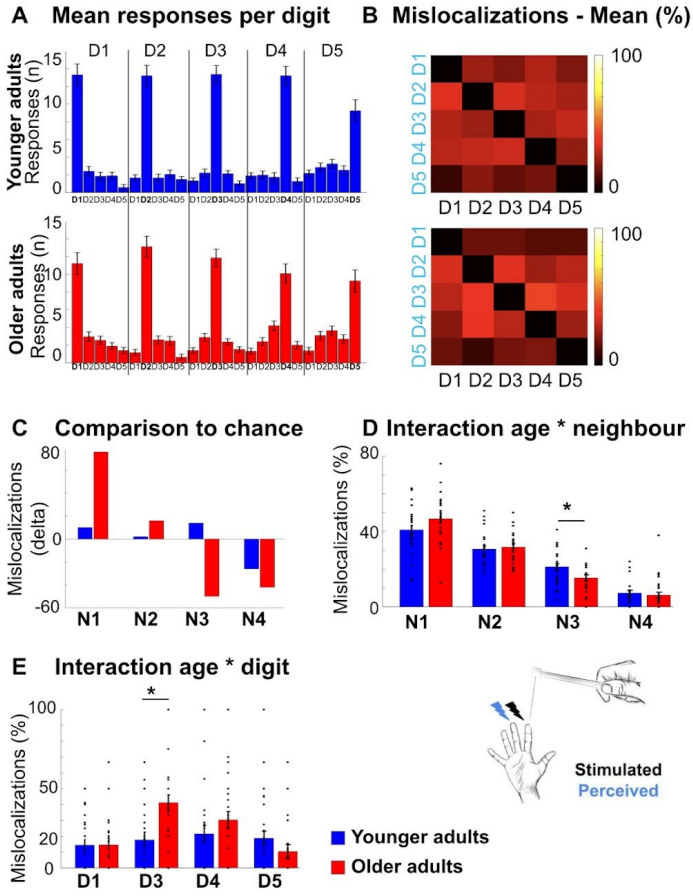

Figure 6. Mislocalizations reflect representational similarity of topographic fields and adjacency of cortical representations. A,B: Finger-specific responses to digit stimulation in younger and older adults shown as numbers of responses per digit dependent on stimulated digit (stimulated digit shown at *top row*, **A**) and as relative distribution of mislocalizations (**B**) (mean ± SE). in **B**, X-axes represent stimulated digits, y-axes represent response digits. See **Supplemental Figure 6** for hit rates and response biases. **C:** Difference values between the measured distribution of mislocalizations and the distribution as expected by chance for both age groups. The mislocalizations were summed for the fingers according to their distance to the stimulated finger. Raw values are shown in **Supplemental Figure 4**. **D:** Distribution of mislocalizations dependent on neighbour (N1-N4) and age group (mean ± SE and individual data)**. E:** Distribution of mislocalizations for D2 stimulations to each digit (mean ± SE and individual data). For complete statistics for each digit (D1-D5) see **Supplemental Figure 5**. * indicates significant difference at *post hoc* *t*-test at an alpha level of $p<.05$. Shown are data of n=25 younger adults and n=25 older adults.

To investigate whether the above-described age-related differences in perceptual finger confusion were due to finger-specific differences in sensitivity or bias (for example, lower sensitivity or higher bias in D2/D3 in older compared to younger adults), we applied signal

detection theory and determined d' and bias by calculating the amount of times a specific finger was touched but not detected (miss), was touched and detected (hit), was not touched but falsely detected (false alarm), or was not touched and not detected (correct rejection). We calculated an ANOVA with the factors age and digit on d' and a robust ANOVA with the same factors on bias. For d', there was no main effect of digit ($F(4,192)=1.16$, $p>.3$), a trend towards a main effect of age ($F(1,48)=3.37$, $p=.073$), with older adults showing lower d' compared to younger adults (older: M=1.36±0.12, younger: M=1.67±0.12), but, critically, there was no interaction between age and digit ($F(4,192)=0.45$, $p>.7$).

For bias, there was a main effect of digit ($F(4, 21.69)=3.54$, $p<.05$), which was due to lower bias for D2 compared to D1 ($t(48.78)=2.46$, $p<.05$), for D2 compared to D5 ($t(39.41)=3.68$, $p<.001$) and for D3 compared to D5 ($t(35.06)=2.93$, $p<.01$) across age groups, no main effect of age ($F(1,24.66)=0.67$, $p>.4$), and, critically, no interaction between digit and age ($F(4,21.69)=0.91$, $p>.4$, see **Supplemental Figure 6** for complete statistics and a graphical overview). The specific difference in perceptual confusion between D2 and D3 in older adults can therefore likely not be assigned to finger- and age-specific differences in d' or bias.

Impaired hand dexterity in older adults

Besides characterizing the participants in functional map features and perceptual digit confusion, we also tested them in three tasks that assessed individual differences in hand dexterity. These tests required coordinated finger movements via the precision grip, and were performed to answer the critical question of how the observed differences in cortical 'de-differentiation' and their perceptual correlates are relevant for everyday hand use. The tests required participants to quickly move small round (Purdue Pegboard Test) or grooved (Grooved Pegboard Test) pins into corresponding holes, or to quickly pick up three small sticks at a time, and place them into a small hole (most difficult task, O'Connor Dexterity Test, see **Fig. 1**). These tests are successful in predicting skills relevant for everyday life, such as picking up and placing small parts, and are standard measures in clinical practice to detect deteriorated movement skills such as in increasing age or in neurodegenerative diseases (Carment et al., 2018; Darweesh et al., 2017; Feys et al., 2017). Hand dexterity was significantly worse in older participants compared to younger participants in all three tests: Older adults were slower than younger adults to complete the Purdue Pegboard Test (older: 79.20s±3.00s, younger: 59.84s±1.49s, $t(35.18)=5.77$, $p<.001$), older adults were slower than younger adults to complete the Grooved Pegboard Test (older: 86.80s±2.47s, younger: 63.84s±1.47s, $t(39.07)=7.98$, $p<.001$), and older adults completed less holes compared to younger adults in the O'Connor Dexterity Test (older: 26.73±1.55, younger: 36.17±1.63, $t(44)=-4.18$, $p<.001$). There was a significant positive correlation between the time (in s) taken to complete the Grooved Pegboard Test and individual age in older adults, and a trend towards a positive correlation between the time (in s) taken to complete the Purdue Pegboard Test and individual age in older adults (see **Supplemental Figure 1** for complete statistics).

Relation between functional map architectures and behavioral phenotypes

Critically, individual differences in hand dexterity in the group of older adults allowed us to ask whether observed age-related changes in topographic map architecture and their perceptual correlates related to better or worse hand dexterity in older adults. This question was evaluated using factor analyses. The aim of factor analysis is to explain the outcome of *n* variables in the data matrix *X* using fewer variables, the so-called *factors*. In order to understand common variances between the above explained differences in hand dexterity and functional as well as perceptual map features, we fitted a model to the data matrix *X* consisting of the following variables: Hand dexterity (Purdue Pegboard Test, Grooved Pegboard Test, O'Connor Dexterity Test), perceptual digit confusion (D2-D3 confusion, N3 confusion), cortical distance (Euclidean distance D2-D3, geodesic distance D2-D3), and representational similarity (N3-finger). The two-factor model (mean psi=.52) loaded performance in the O'Connor Dexterity Test, perceptual digit confusion (D2-D3), and cortical distance (D2-D3, both Euclidean and geodesic) onto *factor 1*, and representational similarity (N3-fingers), performance in the Purdue Pegboard Test, performance in the Grooved Pegboard Test, and perceptual digit confusion (N3) onto *factor 2* (see **Fig. 7A**). The model therefore separated perceptual and functional variables into *local effects* (D2-D3 cortical distance, D2-D3 perceptual confusion, factor 1) and into *global effects* (N3 representational similarity, N3 digit confusion, factor 2, see **Fig. 7A**). Whereas hand dexterity loaded *positively* on age-related *local effects* (more completed holes in O'Connor Dexterity Test for lower cortical distances between D2 and D3, and for higher perceptual confusion between D2 and D3 that both characterize older adults), hand dexterity loaded *negatively* on age-related *global effects* (more time spent on Purdue Pegboard Test and more time spent on Grooved Pegboard Test for lower representational similarity between N3-digits, and lower perceptual confusion to N3 that both characterize older adults).

This overall picture remained the same when we fitted a three-factor model, with the difference that representational similarity was identified as a separate factor (see **Fig. 7C**). When we fitted a four-factor model, the factor specifications remained the same, with the difference that perceptual digit confusion (D2-D3) was fitted as a separate factor. These results show that representational similarity and D2-D3 digit confusion share less common variance with the other variables in their factor. This was also reflected in the correlation analyses, where we see lowest *r*-values for these two variables (see **Fig. 7B**). Taken together, the factor analyses indicate that cortical map features that characterize the full topographic map area can be differentiated from those that only cover parts of the map. The correlation analyses further show that 'more de-differentiation' of local map features relate to better rather than worse hand dexterity as revealed in the (most difficult) O'Connor dexterity test.

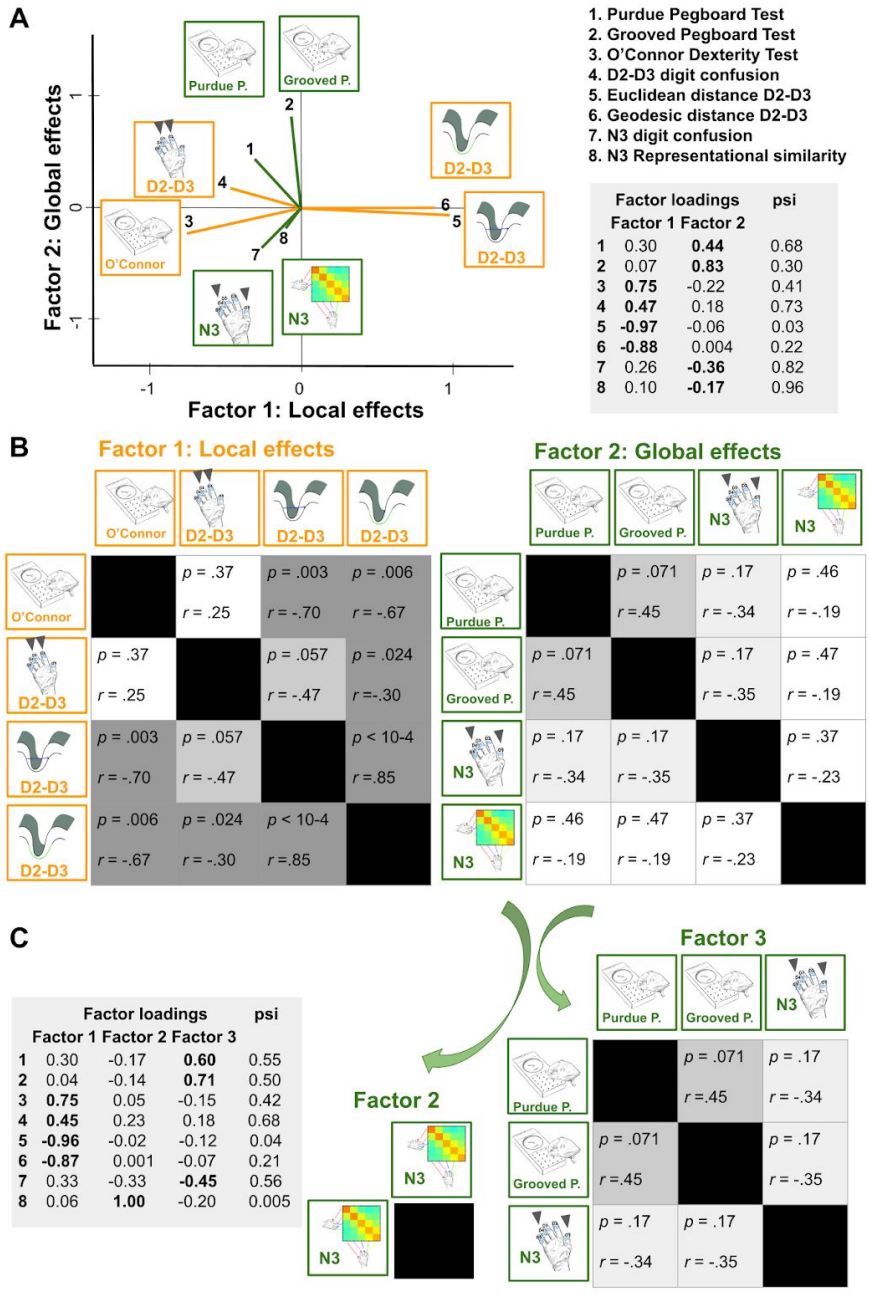

Figure 7. Relation between functional map architectures and behavioral phenotypes. A,B: With a two-factorial model, the data were categorized into features that link to local effects (perceptual confusion between D2 and D3, cortical distance between D2 and D3, factor 1) and those that link to global effects (perceptual confusion to N3, representational similarity to N3, factor 2). Whereas manual dexterity loaded positively onto age-related local effects (higher values in O'Connor test, which reflect better performance, relate to higher perceptual confusion between D2 and D3, and lower cortical distance between D2 and D3), manual dexterity loaded negatively onto global effects (higher values in Purdue and Grooved Pegboard Test, which reflect worse performance, relate to lower perceptual confusion between N3, and lower representational similarity of N3). **A:** factor loadings and psi values, **B:** *p*-values and correlation coefficients (*r*) of Pearson correlations. **C:** Results of three-factorial model. Shown are data of n=17 older adults.

Discussion

Here, we used a combination of ultra-high resolution functional magnetic resonance imaging, computational modeling, psychophysics, and everyday task assessments to detect and describe 'de-differentiated' cortical maps in primary somatosensory cortex (SI) and their association to functional readouts and everyday behavior. Older adults are an ideal population to study mechanisms of cortical de-differentiation, because their topographic map architecture is assumed to become 'less precise' with increasing age, which has been related to maladaptive behavior (Cabeza, 2002; Cassady et al., 2020; Dennis and Cabeza, 2011; Heuninckx et al., 2008; Mattay et al., 2002; Reuter-Lorenz and Lustig, 2005; Riecker et al., 2006).

We did not detect significant differences in basic map statistics such as topographic map size, amplitude and stimulus-related noise between younger and older adults' SI maps. Rather, we observed larger pRF sizes and lower representational similarity between distant fingers on the global level, and reduced cortical distances between the representations of the index finger and the middle finger on the local level. Local and global changes in map topography reflected the pattern of perceptual finger confusion, because older adults showed lower perceptual confusion between distant fingers and higher perceptual confusion between the index and the middle finger compared to younger adults. Because the latter result correlated with better hand dexterity, local cortical 'de-differentiation' was here related to better hand performance in everyday life. These results are in three respects novel and even surprising.

Age-related differences in receptive field sizes in rats are restricted to the hindpaw representation and do not occur in the forepaw representation, with more intensive use of the forepaw compared to the hindpaw assumed to be the underlying reason (David-Jürgens et al., 2008; Godde et al., 2002). In older rats, receptive fields in the hindpaw representation are less inhibitory and larger than receptive fields in younger rats (David-Jürgens et al., 2008; Godde et al., 2002; Spengler et al., 1995), which relates to worse walking behavior (Godde et al., 2002). This topographic pattern could not be replicated for humans, because we here found larger pRF sizes in the hand area of older compared to younger participants, which corroborates the above described hindpaw-selective changes in rats. Other than in rats, we also do not see a significant correlation between larger pRF sizes and worse motor control of the hand, neither for tasks on finger individuation nor for measures of hand dexterity. In addition, we do not see an increase in topographic map amplitude or topographic map size in older adults, which corroborates the idea of an 'overactivated' map in older adults. Our data therefore confirm changes in the inhibitory topographic architecture in older adults' SI area that may explain the increased pRF size (Lenz et al., 2012; Pleger et al., 2016), but leave open the question to which extent these changes are behaviorally relevant, and also question their necessary link to higher BOLD responses in the affected area.

The second finding that was not expected based on prior evidence is the reduced rather than enhanced representational similarity between finger representations in older compared to younger participants. The presumably more de-differentiated cortical maps were in fact less

de-differentiated in distant finger representations. It was even more astonishing that this effect related to a behavioral phenotype, because those fingers that showed less representational similarity in older adults were also mixed up less perceptually. So far, research has stressed that de-differentiated topographic maps are characterized by less rather than more distinct map organization (Cassady et al., 2020; Pleger et al., 2016). However, subcortical U-fibers, which are located within the cortex or in the very outer parts of the subcortical white matter, particularly connect adjacent but not directly neighbouring representations in the cortex. Short-association fibers are among the last parts of the brain to myelinate, and have very slow myelin turnover (Reiser et al., 2007). Myelination and protracted maturation of short-association fibers can continue until the age of fifty (Wu et al., 2016). Fully myelinated U-fibers in older adults and less myelinated U-fibers in younger adults may explain higher correlated short-distance representations in older adults, and good performance in discriminating non-neighbouring signals. This finding hints towards potentially better 'abstract encoding' in older adults, here defined as the distinct extraction of information from adjacent but not neighbouring topographic units.

Perhaps the most surprising finding of our study, however, is the reduced cortical distance between the index and middle finger representations in older adults with preserved map size, where, previously, greater distances between fingers and larger map sizes were reported (Kalisch et al., 2009). Whereas the reduced cortical distance between neighbouring fingers is in principle in line with a de-differentiation model of topographic map architecture, its relation to better rather than worse hand dexterity is certainly not. These findings highlight the importance of combining laboratory measures of perceptual precision with complex everyday task assessments that detail the relevance of fine-grained topographic map changes for everyday hand use. Interestingly, the reduced cortical distance between index and middle finger representations in older adults explains the increased enslaving of the middle finger during index finger flexion in older adults (Van Beek et al., 2019), and may relate to use-dependent plasticity (Makin et al., 2013a). During everyday hand movements, the index and the middle finger correlate less with each other than other neighbouring fingers (Belić and Faisal, 2015), and the index finger is the most independent of the four fingers (Ingram et al., 2008). During tactile learning, plasticity transfers more from the middle finger to the index finger than from the middle finger to the ring finger (Dempsey-Jones et al., 2016). The observed local map changes may therefore either be induced by the correlated input of the middle and ring finger or ring finger and small finger (Kolasinski et al., 2016b), or by age-related changes in the local myeloarchitecture that link to functional map topography (Carey et al., 2018; Kuehn et al., 2017a). In either way, a positive relationship between increased cortical de-differentiation and impairments in everyday hand use is not supported by our data.

Taken together, both in the case of cortical distance, where more local 'de-differentiation' related to better hand dexterity, and in the case of representational similarity, where presumably more 'de-differentiated' cortical maps showed less representations similarity at distant locations, a simple de-differentiation model of cortex function does not seem to appropriately reflect the empirical data. In our view, topographic maps should be classified according to specific map

features that take into account spatial extent (global versus local map changes) and functional readout (integration versus separation). This distinction facilitates the precise investigation of how specific map features relate to corresponding functional readouts such as cortical integration or cortical separation (see **Fig. 1**). For example, whereas reduced cortical distances may increase the local integration of cortical signals, this may benefit tasks that require coordinated finger movements but may worsen tasks that require finger individuation. The distinction between local and global map features is particularly relevant when distinguishing between use-dependent and age-dependent topographic map plasticity, and between adaptive versus maladaptive plasticity. In our data, the local shifts of the index and middle finger representations towards each other seem to have adaptive consequences, whereas maladaptive consequences for global changes in pRF sizes were not identified.

This approach sheds new light on future interventions and training paradigms that aim at speeding up, slowing down, or reversing neuroplastic processes in the cortex. Repeated sensory stimulation of the skin induces NMDA-dependent Hebbian plasticity at the corresponding cortical territory, a mechanism that improves local spatial discrimination thresholds (Dinse et al., 2003; Kuehn et al., 2017b). Synchronous stimulation of more than one finger, but also glueing of multiple fingers, has been used to induce neuroplastic processes of topographic map architectures (Kalisch et al., 2008; Kolasinski et al., 2016b). Synchronous stimulation of all five fingers causes less mislocalizations to nearby digits and more mislocalizations to distant digits (Kalisch et al., 2008, 2007), whereas temporal gluing of the index finger to the middle finger induces a shift of the ring finger towards the small finger, accompanied by less cortical overlap between the middle and the ring finger. This intervention also caused lower thresholds in temporal order judgments between the middle finger and the ring finger, and higher thresholds in temporal order judgments between the ring finger and the small finger (Kolasinski et al., 2016b). Integrating previous knowledge with our data leads to the assumption that concurrent stimulation of *distant* but not neighbouring topographic units and/or correlated input to topographic units that neighbour the affected ones (here the *ring finger and small finger* instead of the index finger and the middle finger) may be particularly beneficial to induce adaptive neuroplasticity in aging topographic maps. This principle can be applied to other cases of distorted (Saadon-Grosman et al., 2015) or preserved (Makin et al., 2013b) map architectures in clinical cases. At a more abstract level, these data indicate that a precise characterization of local and global map changes and their relation to mechanisms of signal integration and separation is a prerequisite for the development of beneficial and individualized training strategies that aim at stopping or reversing maladaptive topographic map change.

In summary, we here provide a comprehensive description of ‘de-differentiated’ topographic maps in SI, and detail the topographic map features that relate to cortical aging. Our data may inspire future research on cortical plasticity, and may motivate the distinction between local and global changes of the map area in relation to functional readout that may either benefit integration or separation of neuronal representations. Future ultra-high field fMRI studies with larger cohorts will uncover global topographic map features and their relation to behaviorally-relevant neuroplasticity.

Materials and Methods

Participants

We tested n=25 younger adults (mean age 25±0.49, ranging from 21 to 29 years, 13 male and 12 female) and n=25 older adults (mean age 72.2±0.81, ranging from 65 to 78 years, 13 male and 12 female) for sensorimotor behavior at the right hand (sample size for touch thresholds, tactile mislocalization and pegboard test based on Kalisch et al., 2008, sample size for topographic shift based on Kalisch et al., 2009). Participants were recruited from the database of the DZNE Magdeburg. Due to the strict exclusion criteria for 7T-MR measurements (see below), participant recruitment and testing took 4 years in total (2016-2020). The Montreal Cognitive Assessment (MOCA) was used as a screening tool to assess the possibility of mild cognitive dysfunction amongst participants. Inclusion criteria were (i) no medication that influenced the central nervous system, (ii) intact hand function (sensory and motor), (iii) 7T-MRI compatibility (see below), and (iv) no sign of early dementia (note that n=1 older adult had a MOCA score of 21; he showed good performance in all tests and was included in the analyses). The MOCA score of the other participants ranged between 25 and 30 (M=28.44±0.25).

We reinvited participants for one 3T-MRI session and one 7T-MRI session. Before the behavioral tests, participants were already screened for 7T-MRI exclusion criteria such as metallic implants and other foreign bodies, active implants (e.g., pacemaker, neurostimulators, cochlear implants, defibrillators and pump system), permanent makeup, tinnitus or hearing impairments. Due to changes in health conditions between the behavioral and MR-measurements, and/or due to stricter MR-regulations due to COVID-19 that were implemented in March 2020, we could reinvite n=20 younger adults and n=18 older adults of the original cohort for the MRI measurements. For n=1 younger adult and n=1 older adult, the 7T-MRI session could not be completed successfully. Therefore, MR analyses are presented for n=19 younger adults (10 female, 9 male, mean age: 24.89 years), and n=17 older adults (8 female, 9 male, mean age: 69.12 years). All participants were paid for their attendance and written informed consent was received from all participants. The study was approved by the Ethics committee of the Otto-von-Guericke University Magdeburg.

General procedure

Participants were invited to three appointments. There was one appointment for behavioral tests, one appointment for a 7T-fMRI session, and one appointment for a 3T-MRI session (see **Fig. 1** for an overview).

Digit confusion

The behavioral tests took place on the first testing day. To estimate perceptual digit confusion, a tactile finger mislocalization task was used (Schweizer et al., 2001, 2000) that is assumed to reflect SI map topography (Kalisch et al., 2008, 2007; Schweizer et al., 2001). First, the detection threshold of each finger was estimated. During testing, participants sat on a chair with the hand positioned palm upwards on a foam cushion. The tested hand was occluded from view. Participants heard white noise through headphones during the task. Before the experiment started, five points were marked on the participant's fingertips via a felt-tip pen: one

point at the center of the volar surface of the first segment of each digit (D1-D5). The detection threshold was estimated for each finger separately with a two-alternative forced choice task. For each finger, mechanical forces were applied to the marked area of the fingertip using Semmes Weinstein monofilaments (Semmes-Weinstein monofilaments; Baseline R, Fabrication Enterprises Inc., White Plains, NY, USA, applied weights: 0.008 g, 0.02 g, 0.04 g, 0.07 g, 0.16 g, 0.4 g, 0.6 g, 1.0 g, 1.4 g, 2.0 g, 4.0 g, 6.0 g). These calibrated filaments assert the same amount of pressure once the filament is bent. Stimulation duration was 1 second. At each trial, two intervals were presented with only one of them containing a stimulation. Participants were asked to detect the stimulation interval by pressing the respective key on the keyboard in a self-paced manner ("1" or "2"). For stimulus application, the experimenter followed auditory instructions via headphones. Neither the hand nor the experimenter were visible to the participant during testing. A randomized sequence (different for each participant) was used to determine which interval contained the stimulation. The adaptive thresholding procedure followed a 3-down/1-up staircase algorithm. Two such staircases were used in an alternating manner, one started at 0.4 g, the other at 0.02 g. The threshold was estimated if the standard deviation from the mean in stimulus intensity was equal or less than 1 step (Gescheider et al., 1996). This was repeated five times, once per finger, in a randomized sequence. The task took approximately 60 to 75 minutes.

After a short break, the finger mislocalization task was applied using Semmes Weinstein monofilaments. The stimulation sites were the same as for the tactile detection task (marked area at fingertip, see above). For each finger, the applied force matched the respective tactile detection threshold as assessed before. Therefore, both younger and older adults were stimulated at each finger at their individual tactile detection threshold, controlling for individual and finger-specific variability in tactile sensitivity. Each trial started with a 3 second stimulation interval, where stimulation was applied to one of five possible fingertips. Stimulation duration was 1 second. The beginning and end of this interval were marked by computer-generated tones. In this five-alternative-forced-choice test, participants were provided with 7 seconds time to verbally name the finger where they felt the touch. Previous studies showed similar tactile misattributions for verbal versus motor responses (Badde et al., 2019). This long response interval was chosen to prevent speed-accuracy trade-offs for older compared to younger adults. If participants did not feel touch at none of the fingers (note that touch was applied at individual thresholds and was therefore expected to be perceived in only around 50% of the cases), they were motivated to name their best guess. The next trial started once the experimenter had inserted the response into the computer. Each finger was stimulated 20 times, stimulation order was pseudo-randomized for each participant in a way that there was maximally one repetition in each sequence. All testing was done by one of the authors (A.C.). Because the results of this task are stable across multiple runs (Schweizer et al., 2000), all testing was done within one session. The task took approximately 20 minutes.

Hand dexterity

Three standard tests were then used to test individual levels of hand dexterity (similar to Kalisch et al., 2008). The *Purdue Pegboard Test* is composed of two rows of 25 small holes each, and

one larger hole at the top that contains 25 small metal pins. The task was to pick one pin at a time with the right hand, and insert them into the holes on the right side of the board from top to bottom. If one of the metal pins dropped during the manual transfer, participants were instructed to continue with the next one. We measured the time to complete the test (in s), and the number of dropped pins (n). The *Grooved Pegboard Test* is composed of a 5x5 matrix of small (grooved) holes, and one larger hole at the top that contains 31 small metal pins. The task was to pick one pin at a time with the right hand, and insert them into the holes from left to right. Other than the Purdue Pegboard Test, this task requires changing the orientation of the pins such that they fit into the grooved holes (shown schematically in **Fig. 1**). If one of the metal pins dropped during the manual transfer, participants were instructed to continue with the next one. We measured the time to complete the test (in s), and the number of dropped pins (n). The *O'Connor Finger Dexterity Test* is the most difficult test of these three, and is composed of a 10x10 matrix of small holes, and one larger hole at the top that contains 315 small, thin metal sticks. Participants were asked to pick three sticks at a time with their right hand, and place all of them into a small hole, starting from left to right. This required orienting the three pins within one hand in a way that they would fit into the small hole. If one of the metal pins dropped during the manual transfer, they were instructed to continue with the next one. Because there are strong individual and age-related differences in this test, participants were here given 4 minutes time to fill as many holes as possible. We measured the number of holes that were successfully filled with three metal sticks (n) as well as the number of dropped pins (n).

MR sequences

Data were acquired at a whole body 7 Tesla MR scanner (Siemens Healthcare, Erlangen, Germany) in Magdeburg using a 32 Channel Nova Medical head coil. First, a whole-brain MP2RAGE sequence with the following parameters was acquired: Voxel resolution: 0.7 mm isotropic, 240 slices, FoV read: 224 mm, TR=4800 ms, TE=2.01 ms, TI1/2=900/2750 ms, GRAPPA 2, sagittal positioning. Shimming was performed prior to collecting the functional data, and two EPIs with opposite phase-encoding (PE) polarity were acquired before the functional scan. The functional EPI sequence (gradient-echo) had the following parameters: Voxel resolution: 1 mm isotropic, FoV read: 192 mm, TR=2000 ms, TE=22 ms, GRAPPA 4, interleaved acquisition, 36 slices. The same sequence was used for all functional tasks (see below). 3T-MRI data were acquired at the Philips 3T Achieva dStream MRI scanner, where a standard structural 3D MPRAGE was acquired (resolution: 1.0 mm x 1.0 mm x 1.0 mm, TI = 650 ms, echo spacing = 6.6 ms, TE = 3.93 ms, α = 10°, bandwidth = 130 Hz/pixel, FOV = 256 mm × 240 mm, slab thickness = 192 mm, 128 slices).

Physiological data recording

A pulse oximeter (NONIN Pulse Oxymeter 8600-FO) clipped to the index finger of the participant's left hand was used to measure the pulse during functional scanning at the 7T-MRI scanner. Additionally, participants wore a breathing belt to capture respiration. An in-house developed setup was used to digitally record and analyze the physiological data (hardware employing National Instruments USB 6008 module with pressure sensor Honeywell

40PC001B1A). The sampling frequency was set to 200 Hz. Data acquisition started with the MR trigger of each functional run.

fMRI task

Five independently-controlled MR-compatible piezoelectric stimulators (Quaerosys, http://www.quaerosys.com) were used to apply tactile stimulation to the five fingertips of the right hand of younger and older adults while lying in the 7T-MRI scanner (Schweisfurth et al., 2015, 2014, 2011). One stimulator was attached to the tip of each right finger using a custom-build, metal-free applicator that could be fitted to individual hand and finger sizes. Each stimulator had 8 individually-controlled pins arranged in a 2x4 array, covering 2.5x9 mm^2 of skin (see **Fig. 1**). Vibrotactile stimulation was applied to the fingertips at a frequency of 16 Hz (Schweizer et al., 2008). Stimulation intensity of each subject and each finger was adjusted to 2.5 times the individual tactile detection thresholds. To minimize adaptation-related differences in map activity between younger and older adults, two randomly chosen pins were raised once at a time, yielding 16 pin combinations per second (Schweisfurth et al., 2015, 2014, 2011).

Participants first underwent two phase-encoded protocols, and then continued with two blocked-design protocols. The phase-encoded protocols consisted of 2 runs of 20 cycles each. Each cycle lasted 25.6 seconds, stimulation was applied to each fingertip for 5.12 seconds, and for 20 times. Stimulation was delivered either in a forward order (D1->D5) or in a reverse order (D5->D1, see **Fig. 1**). Half of the participants of each age group started with the forward-run, the other half started with the reverse-run. One run comprised 256 scans (512 seconds for a TR of 2 seconds), and lasted for 8 minutes and 31 seconds. Participants were instructed to covertly count short randomly distributed interrupts embedded in the tactile stimulation (duration 180 ms, slightly longer than in Schweisfurth et al., 2015, 2014, 2011 to account for the effect of age). There were the same number of gaps per finger and per person.

The blocked-design paradigm comprised 6 conditions: Stimulation to D1, D2, D3, D4, D5, and a rest condition with no stimulation. The same stimulation protocol as in the phase-encoded design was used (each finger was stimulated for 5.12 seconds, same frequency and stimulation duration). Fingers were here stimulated in a pseudo-random sequence, where there was never one finger stimulated more than two times in a row. In 70% of the trials, there was a 2 second pause between two subsequent stimulations, in 30% of the trials, there was a 6 seconds pause between two subsequent stimulations. This was counterbalanced across fingers. Each finger was stimulated 10 times. One run comprised 208 scans, and lasted for 6 minutes and 56 seconds. The same task was applied as in the phase-encoded paradigm. The blocked-design run was repeated twice. Subsequently, two runs were measured where a one-TR stimulation of all 5 fingers was followed by a 11-TR rest without any stimulation. This sequence was repeated 10 times for each run, with 2 runs in total. Finally, we acquired a 5-minutes resting state scan, where participants were asked to look at a centrally presented fixation cross, and to think about nothing in particular. All functional measurements together took around 40 minutes.

Behavioral analyses: Digit confusion

Using an adaptive staircase procedure, the detection threshold was estimated if the standard deviation from the mean in stimulus intensity was equal or less than 1 step (Gescheider et al., 1996). These values were transformed logarithmically ($\log_{10}$0.1mg), and were used as stimulation intensities for the mislocalization task. Mislocalizations were defined as responses where participants indicated another finger than the one that was stimulated, i.e., as false responses. These were analysed with respect to their distribution across the non-stimulated fingers. Mislocalizations were grouped according to their distance to the stimulated finger into 1st neighbour, 2nd neighbour, 3rd neighbour and 4th neighbour (N1-N4) mislocalizations (e.g., if D2 was stimulated and the participant assigned the touch to D4, this was a N2 mislocalization, if the participant assigned the touch to D5 instead, this was a N3 mislocalization, and so forth, Schweizer et al., 2000). No errors for one specific finger were computed as zero values. The resulting distribution of the relative number of mislocalizations towards N1-N4 was compared to the expected equal distribution of mislocalizations for each finger using the *G*-test of goodness of fit (Sokal and Rohlf, 1981). An equal distribution is expected if the naming of the localization is at chance level and does not follow the principles of topographic arrangement, where more mislocalizations are expected to closer neighbours compared to distant neighbours (Schweizer et al., 2001, 2000). In this analysis, the different distributions of response options for the different neighbours were taken into account (i.e., the fact that across all fingers, there are more response options for 1st compared to 2nd, 2nd compared to 3rd, and 3rd compared to 4th neighbour) (Schweizer et al., 2000). The *G*-tests of goodness of fit were Holm-Bonferroni corrected at a significance threshold of $p<.05$.

To calculate hit rates, for each participant, the number of correctly perceived stimulus locations was accumulated for each finger and divided by the number of stimulations of that finger. This resulted in the proportion of correct responses (hit rates) in percent for each finger. False alarms were defined as the number of times that this same finger was falsely identified as the one being stimulated when actually not touched. This is irrespective of which finger was touched that time (i.e., it could be misclassified when N1, N2, N3 or N4 was touched). For the estimation of *d'*, hits and false alarms were first converted to *z*-scores. The false alarm *z*-scores were then subtracted from the hit rate *z*-scores, and the sensitivity index was obtained for each finger separately. The beta criterion (bias) was further calculated for each finger based on the *z*-scores by estimating the exponential of the difference between the false alarm *z*-scores and the hit rate *z*-scores, each raised to a power of two, and divided by 2. To overcome the problem of missing events, the loglinear transformation was applied to the analyses (Stanislaw and Todorov, 1999).

The distribution of mislocalizations (in %) was used for an ANOVA with the factors neighbour (N1-N4) and age (young, old). To test for finger-specific effects, an ANOVA was calculated for each digit with the factors response digit and age (young, old). For D1, response digit was specified as D2, D3, D4, D5; for D2, it was specified as D1, D3, D4, D5, and so forth. To estimate whether age-dependent changes in mislocalizations are due to age-related differences in sensitivity and/or bias, two ANOVAs with the factors digit (D1-D5) and age (young, old) were also conducted for sensitivity and bias. In the case of sensitivity, the sensitivity index *d'* was

used as a dependent variable and in the case of bias, the beta criterion was used as a dependent variable. Robust ANOVAs were calculated if the distribution of values in the non-normality distributed data was skewed, ANOVAs were calculated if the data were normally distributed, or if only sub-groups of the data were not normally distributed (Glass et al., 1972; Harwell et al., 1992; Lix et al., 1996). Robust ANOVAs based on trimmed means were computed in R (R Core Team, 2019) with the statistical package WRS2, developed by Wilcox, and the function 'bwtrim'. Trimmed means are formed after the removal of a specific percentage of scores from the lower and higher end of the score distribution, obtaining thus accurate results even for non symmetrical distributions, by removing outliers and skew (Field, 2009). As *post hoc* tests for the ANOVA, independent-sample *t*-tests were computed, as *post hoc* tests for the robust ANOVA, the Yuen-Welch method for comparing 20% trimmed means was applied, which is a robust alternative to independent samples *t*-test (Mair and Wilcox, 2020). The latter test was computed by using the function 'yuen' of the WRS2 package in R. An alpha level of $p<.05$ was used to test for significant main effects and interactions.

Behavioral analyses: Hand dexterity

For the Purdue Pegboard Test and the Grooved Pegboard Test, the time (in s) taken to complete each test was compared between the two age groups using two independent sample *t*-tests. For the O'Connor Finger Dexterity Test, the number of successfully filled holes (n) was compared between the two age groups using one independent sample *t*-test. A Bonferroni-corrected alpha level of $p<.016$ was used to test for significant group differences.

MRI analyses

Surface reconstruction

FSL 5.0 (Smith et al., 2004; Woolrich et al., 2009) and Freesurfer's recon-all (http://surfer.nmr.mgh.harvard.edu/) were used for brain segmentation and cortical surface reconstruction using the T1-weighted 3D MPRAGE. Note that the spatial resolution of the T1-weighted MPRAGE that was used for brain segmentation and the functional EPI sequence was identical (1mm isotropic). Recon-all is a fully automated image processing pipeline, which, among other steps, performs intensity correction, transformation to Talairach space, normalization, skull-stripping, subcortical and white-matter segmentation, surface tessellation, surface refinement, surface inflation, sulcus-based nonlinear morphing to a cross-subject spherical coordinate system, and cortical parcellation (Dale et al., 1999; Fischl et al., 1999). Skull stripping, construction of white and pial surfaces, and segmentation were manually checked for each individual participant.

Preprocessing

Motion artefacts and compressed distortion can be a serious problem for functional MR data, particularly those acquired at 7T where field inhomogeneity is increased. To resolve these problems, two EPIs with opposite phase-encoding (PE) polarity were acquired before the functional scan. A point spread function (PSF) mapping method was applied to perform distortion correction of both EPIs with opposite PE polarity (In et al., 2016). PSF mapping allows

reliable distortion mapping due to its robustness to noise and field inhomogeneity (Robson et al., 1997). Because the amount of spatial information differs between the opposite PE datasets, a weighted combination of the two distortion-corrected images was incorporated to maximize the spatial information content of the final, corrected image. The EPI-images of the functional blocks were motion corrected to time-point=0, and the extended PSF method was applied to the acquired and motion-corrected images to perform geometrically accurate image reconstruction. Finally, after data acquisition, slice timing correction was applied to the functional data to correct for differences in image acquisition time between slices using SPM8 (Statistical Parametric Mapping, Wellcome Department of Imaging Neuroscience, University College London, London, UK).

Functional time series were then registered to the T1-weighted 3D MPRAGE used for recon-all using csurf tkregister (12 degrees of freedom, non-rigid registration). The resulting registration matrix was used to map the x,y,z location of each surface vertex into functional voxel coordinates. The floating point coordinates of points at varying distances along the surface normal to a vertex were used to perform nearest neighbour sampling of the functional volume voxels (i.e., the 3D functional data were associated with each vertex on the surface by finding which voxel that point lay within). Because time series of the different cycle directions (D1->D5 and D5->D1) were mirror-symmetric to each other, they were averaged time point by time point by reversing the direction of time on a scan-by-scan basis. The time-reversed cycle direction (D5->D1 cycle) was time-shifted before averaging by 4 seconds (= 2 TRs) to compensate for hemodynamic delay. Averaging was done in 3D without any additional registration. Note that data were neither normalized nor smoothed (beyond interpolation during registration) during this procedure.

Moreover, physiological fluctuations originating from cardiac pulsation and respiration are considered a primary source of noise in functional MR data sets, particularly for resting state data acquired at high field strengths (Krüger and Glover, 2001). The resting-state functional data were therefore corrected for pulse- and respiration-induced noise. To prepare the physiological data for noise correction and to remove acquisition artifacts, we used the open-source Python-based software ‘PhysioNoise’ (Kelley et al., 2008). Resulting respiratory and cardiac phase data were then used to correct the resting-state time series for pulse- and respiration-induced noise by performing RETROspective Image CORrection (RETROICOR) (Glover et al., 2000) on a slice-by-slice basis (Birn et al., 2006). Residuals were taken as cleaned data to regress out motion-related noise parameters (extracted from the raw data) using the program vresiduals implemented in LIPSIA (freely available for download at: github.com/lipsia-fmri/lipsia). Finally, the data were high-pass filtered at 0.01 Hz (allowing frequencies faster than 0.01 Hz to pass) using the program vpreprocess implemented in LIPSIA. For n=9 participants, physiological data could not successfully be acquired due to a loss of the pulse oximeter and/or loosening of the breathing belt during scanning, which interrupted successful physiological data sampling. For n=4 participants, we observed severe motion artifacts for the resting state data. Therefore, resting state analyses are presented for a subset of participants only (n=12 younger and n=12 older adults).

Phase-encoded analyses

The program Fourier implemented in csurf (http://www.cogsci.ucsd.edu/~sereno/.tmp/dist/csurf) was used to conduct statistical analyses on the averaged individual time series of the averaged forward- and reversed-order runs (Kuehn et al., 2018). Csurf was used to run discrete Fourier transformations on the time course at each 3D voxel, and then calculates phase and significance of the periodic activation. There were 20 stimulation cycles, which were used as input frequencies. No spatial smoothing was applied to the data before statistical analyses. Frequencies below 0.005 Hz were ignored for calculating signal-to-noise, which is the ratio of amplitude at the stimulus frequency to the amplitudes of other (noise) frequencies. Very low frequencies are dominated by movement artifacts, and this procedure is identical to linearly regressing out signals correlated with low frequency movements. High frequencies up to the Nyquist limit (1/2 the sampling rate) were allowed. This corresponds to no use of a low-pass filter. For display, a vector was generated whose amplitude is the square root of the F-ratio calculated by comparing the signal amplitude at the stimulus frequency to the signal at other noise frequencies and whose angle was the stimulus phase. The data were then sampled onto the individual freesurfer surface. To minimize the effect of superficial veins on BOLD signal change, superficial points along the surface normal to each vertex (upper 20% of the cortical thickness) were disregarded. The mean value of the other layers (20-100% cortical depth) were used to calculate individual maps. On the individual subject level, clusters that survived a surface-based correction for multiple comparisons of $p<.01$ (correction was based on the cluster size exclusion method as implemented by surfclust and randsurfclust within the csurf FreeSurfer framework (Hagler et al., 2006)), and a cluster-level correction of $p<.001$, were defined as significant. On the group level, clusters that survived a cluster-filtered correction of the F-values were considered significant (pre-cluster statistical threshold of $p<.01$, and minimum surface area of 14 mm^2, according to Hagler et al., 2007).

Complex-valued data from each individual subject's morphed sphere were also sampled to the canonical icosahedral sphere (7th icosahedral sub-tessellation) surface. For each target vertex, the closest vertex in the source surface was found. The components in this coordinate system were then averaged (separately for younger and older adults' brains), and the (scalar) cross-subject F-ratio was calculated. The cross-subject F-ratio is calculated based on the complex coefficients at the stimulus frequency from each subject. The F-ratio is described as follows:

$$\frac{[xav^2 + yav^2]/2}{[Sum(\_x-xav)^2)/n + Sum(\_y-yav)^2/n] / [2*n-2]}$$

where _x and _y are the raw Fourier coefficients at the stimulus frequency, xav and yav are the average of them, and n is the number of subjects. This is described and demonstrated in Hagler et al., 2007. A cluster threshold of $p<.01$ was defined as significant.

Surface-based masks of area 3b of each individual brain were used to define area 3b. Surface area measurements were extracted by calculating the sum of ⅓ of the area of each of the triangles surrounding that vertex. Surface area was defined as the summed vertex-wise area of the significant area 3b map. We report two sums: the surface area as of the individual surface (the .area field), and the surface area of the original surface (the lh.area file). F-values of the Fourier model from the significant tactile map area in area 3b were extracted subject-by-subject, and were then averaged. To estimate mean response amplitudes of the tactile maps (in %), we estimated the discrete Fourier transform response amplitude (hypotenuse given real and imaginary values) for each vertex within the significant map area. This value was multiplied by 2 to account for positive and negative frequencies, again multiplied by 2 to estimate peak-to-peak values, divided by the number of time points over which averaging was performed (to normalize the discrete Fourier transform amplitude), and divided by the average brightness of the functional data set (excluding air). Finally, the value was multiplied by 100 to estimate percentage response amplitude (Kuehn et al., 2018). Independent-sample *t*-tests with a Bonferroni-corrected alpha level of $p<.0125$ were used to compare mean F-values, mean & response amplitude, and mean surface area (current and original surface) between younger and older adults. The chi-square goodness-of-fit test was used to test for normality of the data.

Consistency of map alignment

We estimated the vertex-wise consistency of the map gradient within each age group using the dispersion index *d*, which is described as follows:

$$d = \frac{\text{amplitude of vector average}}{\text{average amplitude of indiv vectors}}$$

This index is 1.0 in the case of perfectly aligned vectors across the entire group (within younger or within older participants), independent of vector amplitude. *d* therefore distinguishes a vector average that was generated by a set of large but inconsistent signals (lower *d*) from a same-sized vector average that was generated by a set of smaller but more consistent signals (higher *d*). As such, *d* provides an indication about the consistency of the map alignment within each age group.

GLM analyses

Fixed-effects models on the 1st level were calculated for each subject separately using the general linear model (GLM) as implemented in SPM8. The analyses were performed on the two blocked-design runs (run 3 and run 4 of the experiment). Because we treated each finger individually and independently, BOLD activation elicited by each finger's tactile stimulation was treated as an independent measure in the quantification (Kuehn et al., 2018; Stringer et al., 2014). We modeled one session with five regressors of interest each (stimulation to D1, D2, D3, D4, D5). We computed five linear contrast estimates: Touch to D1, D2, D3, D4, and D5 (e.g., the contrast [4 -1 -1 -1 -1] for touch to D1). Frame-to-frame displacement of realignment

parameters (first two shift regressors and rotation regressors) did not differ significantly between age groups (all $p>.5$). Given that functional and anatomical data were not normalized, no group statistics were performed with SPM. Instead, on the individual subject level, voxels that survived a significance threshold of $p<.05$ and $k>3$ were mapped onto the cortical surfaces using the procedure as described above. These thresholded contrast images were used for finger mapping analyses on the individual subject level within the FSL-framework.

Representational similarity analysis

For all participants, beta values were extracted from each single finger receptive area within area 3b. Anterior-posterior boundaries were taken from Freesurfer surface labels. Significant tactile maps in each participant were used to define the response regions. We characterized topographic similarity of finger representations for each digit pair by computing the similarity between all digit combinations between the first and second run within the area 3b map area (Kuehn et al., 2018). Correlation coefficients of the vectors were calculated using Pearson correlations. The correlation coefficients were first computed at the individual subject level, Fisher *z*-transformed, and then averaged across subjects to calculate digit-specific group averaged correlation matrices. We computed an ANOVA with the factors neighbour (N0-N4) and age (young, old) to test for age-related differences in distant-dependent similarities between finger representations between runs. We used an alpha level of $p<.05$ to test for significant main effects and interactions.

Preprocessed resting state data that were corrected for physiological noise (see above) were used to compute similarities between time series of finger representations in area 3b. The matlab-function ‘xcorr’ was used to compute cross-correlations between time series of all finger pairs. Cross-correlations measure the similarity between two vectors and their shifted (lagged) copies as a function of the lag, and take into account temporal shifts as a function of TR. For any given lag, cross-correlations estimate the correlation between two random sequences and estimate functional connectivity (Hyde and Jesmanowicz, 2012).

Cortical distance and cortical overlap

Geodesic distances between receptive fields (in mm) were computed using the Dijkstra algorithm. The path follows the edges of triangular faces on the surface between each peak vertex of each individual receptive area. Distances between neighbouring digit representations were calculated by extracting paths between peaks of neighbouring digit representations. We also calculated Euclidean distances between each neighbouring digit pair. With A(x1,x2,z3) and B(x2,y2,z3) the Euclidean distance were computed as

$$d(A,B) = sqt((x2-x1)2 + (y2-y1)2 + (z2-z1)2))$$

Geodesic and Euclidean distances between each neighbouring digit pair were compared between groups using a 4x2 ANOVA with the factors digit-pair (D1-D2, D2-D3, D3-D4, D4-D5)

and age (young, old). The chi-square goodness-of-fit test was used to test for normality of the data.

Cortical overlap between adjacent digits (D1-D2, D2-D3, D3-D4 and D4-D5) was calculated using the Dice coefficient (Dice, 1945; Kikkert et al., 2016; Kolasinski et al., 2016b). The dice coefficient varies from a value of 0, indicating no digit overlap, to a value of 1, indicating perfect digit overlap. Where A and B are the area of the two digit representations, the Dice Coefficient is expressed as:

$2|A \cap B| / |A|+|B|$

Vertices of digit representations were determined as the number of significant vertices within the tactile 3b map area. The chi-square goodness-of-fit test was used to test for normality of the data. For normally distributed data, an ANOVA was calculated with the factors digit-pair (D1-D2, D2-D3, D3-D4 and D4-D5) and age (young, old). An alpha level of $p<.05$ was used to identify significant main effects and interactions.

Hedges' *g* was used to estimate effect sizes (Hedges, 1981). Hedges' *g* is similar to Cohen's *d* but outperforms Cohen's *d* when sample sizes are low. 95% confidence intervals and Hedges' *g* were computed via bootstrapping 10,000 times. Bootstrapping is a non-parametric statistical test that can be applied both when the data are normal and non-normal distributed. Bootstrapping is particularly suitable for data with small sample sizes. Forest plots were used to visualize effect sizes (https://www.mathworks.com/matlabcentral/fileexchange/71020-forest-plot-for-visualisation-of-multiple-odds-ratios). A forest plot is a graphical display that illustrates the relative strength of interventions, such as training effects, in different conditions (Timm and Kuehn, 2020), and is often used in clinical trials to compare the effectiveness of treatments (e.g., Kang et al., 2016).

Bayesian pRF modeling

Population receptive field (pRF) modeling was performed using the SPM-based BayespRF Toolbox (freely available for download from https://github.com/pzeidman/BayespRF) which is dependent on Matlab (SPM12 and Matlab 2018b). The BayespRF toolbox provides a generic framework for mapping pRFs associated with stimulus spaces of any dimension onto the brain. It was first used for mapping 2-dimensional (2D) visual pRFs in human visual cortex (Zeidman et al., 2018), and it was recently applied to map somatosensory pRFs in human SI (Puckett et al., 2020). Data were prepared for the pRF modeling by reducing the number of voxel time courses. This was achieved by performing a GLM analyses in SPM; only data that passed a significance threshold of $p<.05$ were used for the pRF modeling (Zeidman et al. 2018, Puckett et al. 2018). This procedure allows reducing computing time considerably (note that one pRF modeling process takes around 2 days for the given input data). The resulting mask was combined with the freesurfer mask of area 3b. pRF modeling was then conducted on a voxel-wise basis, where the fit between an estimated waveform and the empirically measured BOLD-response was optimized. This was achieved by modifying the size and position of the pRF model. The

posterior model probability was thresholded at >0.95 (Puckett et al., 2020; Zeidman et al., 2018). We defined the somatosensory space using the same 2D matrix that was used for visual pRF mapping, but with limiting the dimensions to +/- 12.5 in both dimensions. pRF modeling was performed on the x-dimension, i.e., the inferior-superior dimension of topographic alignment. Note that similar to Puckett et al., 2020, these analyses model one dimension in the 2-dimensional sensory space. We allowed the minimal pRF size to be not smaller than 1/10th of the sensory space occupied by a single fingertip, and the maximum size restricted to the equivalence of all five fingers (i.e., 25 units) (Puckett et al., 2020). A Gaussian pRF profile was chosen as a response function for pRF analysis (code available at https://gitlab.com/pengliu1120/bayesian-prf-modelling.git). This model was characterized as a normal, excitatory distribution with pRF center location (x) and width (i.e., σ, the standard deviation of the Gaussian profile) as estimated parameters (Puckett et al., 2020).

After processing, output volumes were extracted from the obtained results, including distance, angle, width, beta, decay, transit and epsilon. Distance and angle are the vectors of polar coordinates depending on stimuli space definition, width is the defined pRF size parameter, ranging from 0.5 to 25. Distance values were used to define locations of activated voxels for each finger, width values were used as pRF size estimates for activated voxels. For display, the dimensions of the pRF distance volumes were adjusted to 0/25.

After performing Bayesian pRF modelling for every subject, group average pRF sizes were calculated and used for statistical analysis. A two-way ANOVA was performed with age and finger as independent variables, and group average pRF size as dependent variable. We also performed correlation analyses between average pRF sizes and cortical distances (Euclidean distance and geodesic distance), mean dice coefficients, recorded time of the Purdue Pegboard Test and recorded time of the Grooved Pegboard Test.

Factor analyses and correlations

We used the function ‘factoran’ in MATLAB_R2014b, which fits factor analysis models using maximum likelihood estimates. We searched for one, two, three, and four common factors, i.e. factors that might affect several of the variables in common. In that way, we obtained maximum likelihood estimates of the factor loadings and the specific variances, representing independent random variability, for each variable. For the refitted models with more than one common factor, the loadings were initially estimated without rotation, but for better interpretability, we further used the ‘promax’ oblique rotation. Factor rotation aimed at obtaining for each variable only a small number of large loadings affected by the factors, preferably only one. The ‘promax’ rotation chosen here rotated the factor axes separately, allowing them to have an oblique angle between them, and computed new loadings based on this rotated coordinate system. We computed lambda as the coefficient, or loading, of the jth factor for the ith variable. Note that for the factor analysis with three and four common factors, some of the specific variances were equal to the value of the 'delta' parameter (close to zero), leading to a fit known as a Heywood case. We computed psi as the specific variance of the model. Psi=1 would indicate that there is *no* common factor component in that variable, while psi=0 would indicate that the variable is

entirely determined by common factors. Correlation coefficients between behavioral measures and functional map features that showed significant differences between age groups were calculated within the group of older adults using Pearson correlations. Correlation coefficients were determined between the following variables: Hand dexterity (Purdue Pegboard Test - recorded time, Grooved Pegboard Test - recorded time, O'Connor Finger Dexterity Test - number of successfully completed holes), perceptual digit confusion (percentage of D2-D3 confusion, percentage of N3 confusion), cortical distance (Euclidean distance between D2 and D3, geodesic distance between D2 and D3), and representational similarity (RS of N3).

Acknowledgments

E.K. was funded by ESIF/EFRE 2014-2020; FKZ: ZS/2016/04/78113, Vorhaben: Center for Behavioral Brain Sciences (CBBS); P.L. and J.D. were funded by the German Research Foundation (Deutsche Forschungsgemeinschaft, DFG) (KU 3711/2-1, project number: 423633679). A.C. was funded by the Else Kröner Fresenius Stiftung (EKFS) (2019-A03).

Competing Interests

The authors declare no competing interests.

Author Contributions

Conceptualization - E.K., T.W.; Formal analyses - E.K., P.L., A.C., J.D.; Funding acquisition - E.K., T.W.; Investigation - E.K.; Supervision - E.K.; Writing - original draft - E.K., P.L., A.C.; Writing - review & editing - J.D., T.W.

References

Amedi A, Raz N, Pianka P, Malach R, Zohary E. 2003. Early “visual” cortex activation correlates with superior verbal memory performance in the blind. *Nature Neuroscience*. doi:10.1038/nn1072

Badde S, Röder B, Heed T. 2019. Feeling a Touch to the Hand on the Foot. *Curr Biol* **29**:1491–1497.

Belić JJ, Faisal AA. 2015. Decoding of human hand actions to handle missing limbs in neuroprosthetics. *Front Comput Neurosci* **9**:27. doi:10.3389/fncom.2015.00027

Birn RM, Diamond JB, Smith MA, Bandettini PA. 2006. Separating respiratory-variation-related fluctuations from neuronal-activity-related fluctuations in fMRI. *Neuroimage* **31**:1536–1548. doi:10.1016/j.neuroimage.2006.02.048

Cabeza R. 2002. Hemispheric asymmetry reduction in older adults: the HAROLD model. *Psychol Aging* **17**:85–100. doi:10.1037//0882-7974.17.1.85

Carey D, Caprini F, Allen M, Lutti A, Weiskopf N, Rees G, Callaghan MF, Dick F. 2018. Quantitative MRI provides markers of intra-, inter-regional, and age-related differences in young adult cortical microstructure. *NeuroImage*. doi:10.1016/j.neuroimage.2017.11.066

Carment L, Abdellatif A, Lafuente-Lafuente C, Pariel S, Maier MA, Belmin J, Lindberg PG. 2018. Manual Dexterity and Aging: A Pilot Study Disentangling Sensorimotor From Cognitive Decline. *Front Neurol* **9**:910. doi:10.3389/fneur.2018.00910

Cassady K, Ruitenberg MFL, Reuter-Lorenz PA, Tommerdahl M, Seidler RD. 2020. Neural Dedifferentiation across the Lifespan in the Motor and Somatosensory Systems. *Cereb Cortex* **30**:3704–3716. doi:10.1093/cercor/bhz336

Crabtree JW. 1992. The Somatotopic Organization Within the Cat’s Thalamic Reticular Nucleus. *European Journal of Neuroscience*. doi:10.1111/j.1460-9568.1992.tb00160.x

Dale AM, Fischl B, Sereno MI. 1999. Cortical surface-based analysis. I. Segmentation and surface reconstruction. *Neuroimage* **9**:179–194. doi:10.1006/nimg.1998.0395

Darweesh SKL, Wolters FJ, Hofman A, Stricker BH, Koudstaal PJ, Ikram MA. 2017. Simple Test of Manual Dexterity Can Help to Identify Persons at High Risk for Neurodegenerative Diseases in the Community. *J Gerontol A Biol Sci Med Sci* **72**:75–81. doi:10.1093/gerona/glw122

David-Jürgens M, Churs L, Berkefeld T, Zepka RF, Dinse HR. 2008. Differential effects of aging on fore- and hindpaw maps of rat somatosensory cortex. *PLoS One* **3**:e3399. doi:10.1371/journal.pone.0003399

Dempsey-Jones H, Harrar V, Oliver J, Johansen-Berg H, Spence C, Makin TR. 2016. Transfer of tactile perceptual learning to untrained neighboring fingers reflects natural use relationships. *J Neurophysiol* **115**:1088–1097. doi:10.1152/jn.00181.2015

Dennis NA, Cabeza R. 2011. Age-related dedifferentiation of learning systems: an fMRI study of implicit and explicit learning. *Neurobiol Aging* **32**:2318.e17–30. doi:10.1016/j.neurobiolaging.2010.04.004

Dice LR. 1945. Measures of the Amount of Ecologic Association Between Species. *Ecology* **26**:297–302. doi:10.2307/1932409

Dinse HR, Ragert P, Pleger B, Schwenkreis P, Tegenthoff M. 2003. Pharmacological modulation of perceptual learning and associated cortical reorganization. *Science* **301**:91–94. doi:10.1126/science.1085423

Feys P, Lamers I, Francis G, Benedict R, Phillips G, LaRocca N, Hudson LD, Rudick R, Multiple Sclerosis Outcome Assessments Consortium. 2017. The Nine-Hole Peg Test as a manual dexterity performance measure for multiple sclerosis. *Mult Scler* **23**:711–720.

doi:10.1177/1352458517690824
Field A. 2009. Discovering Statistics through SPSS:(and sex and drugs and rock'n'roll).
Fischl B, Sereno MI, Dale AM. 1999. Cortical surface-based analysis. II: Inflation, flattening, and a surface-based coordinate system. *Neuroimage* **9**:195–207. doi:10.1006/nimg.1998.0396
Gescheider GA, Edwards RR, Lackner EA, Bolanowski SJ, Verrillo RT. 1996. The Effects of Aging on Information-Processing Channels in the Sense of Touch: III. Differential Sensitivity to Changes in Stimulus Intensity. *Somatosensory & Motor Research*. doi:10.3109/08990229609028914
Glass GV, Peckham PD, Sanders JR. 1972. Consequences of Failure to Meet Assumptions Underlying the Fixed Effects Analyses of Variance and Covariance. *Rev Educ Res* **42**:237–288. doi:10.3102/00346543042003237
Glover GH, Li T-Q, Ress D. 2000. Image-based method for retrospective correction of physiological motion effects in fMRI: RETROICOR. *Magnetic Resonance in Medicine: An Official Journal of the International Society for Magnetic Resonance in Medicine* **44**:162–167.
Godde B, Berkefeld T, David-Jürgens M, Dinse HR. 2002. Age-related changes in primary somatosensory cortex of rats: evidence for parallel degenerative and plastic-adaptive processes. *Neurosci Biobehav Rev* **26**:743–752. doi:10.1016/s0149-7634(02)00061-1
Hagler DJ Jr, Riecke L, Sereno MI. 2007. Parietal and superior frontal visuospatial maps activated by pointing and saccades. *Neuroimage* **35**:1562–1577. doi:10.1016/j.neuroimage.2007.01.033
Hagler DJ Jr, Saygin AP, Sereno MI. 2006. Smoothing and cluster thresholding for cortical surface-based group analysis of fMRI data. *Neuroimage* **33**:1093–1103. doi:10.1016/j.neuroimage.2006.07.036
Harwell MR, Rubinstein EN, Hayes WS, Olds CC. 1992. Summarizing Monte Carlo Results in Methodological Research: The One- and Two-Factor Fixed Effects ANOVA Cases. *J Educ Behav Stat* **17**:315–339. doi:10.3102/10769986017004315
Hedges LV. 1981. Distribution Theory for Glass's Estimator of Effect Size and Related Estimators. *J Educ Behav Stat* **6**:107–128. doi:10.2307/1164588
Heuninckx S, Wenderoth N, Swinnen SP. 2008. Systems neuroplasticity in the aging brain: recruiting additional neural resources for successful motor performance in elderly persons. *J Neurosci* **28**:91–99. doi:10.1523/JNEUROSCI.3300-07.2008
Hintiryan H, Foster NN, Bowman I, Bay M, Song MY, Gou L, Yamashita S, Bienkowski MS, Zingg B, Zhu M, Yang XW, Shih JC, Toga AW, Dong H-W. 2016. The mouse cortico-striatal projectome. *Nat Neurosci* **19**:1100–1114. doi:10.1038/nn.4332
Huber L, Finn ES, Handwerker DA, Bönstrup M, Glen DR, Kashyap S, Ivanov D, Petridou N, Marrett S, Goense J, Poser BA, Bandettini PA. 2020. Sub-millimeter fMRI reveals multiple topographical digit representations that form action maps in human motor cortex. *Neuroimage* **208**:116463. doi:10.1016/j.neuroimage.2019.116463
Hyde JS, Jesmanowicz A. 2012. Cross-correlation: an fMRI signal-processing strategy. *Neuroimage* **62**:848–851. doi:10.1016/j.neuroimage.2011.10.064
Ingram JN, Körding KP, Howard IS, Wolpert DM. 2008. The statistics of natural hand movements. *Exp Brain Res* **188**:223–236. doi:10.1007/s00221-008-1355-3
In M-H, Posnansky O, Speck O. 2016. PSF mapping-based correction of eddy-current-induced distortions in diffusion-weighted echo-planar imaging. *Magn Reson Med* **75**:2055–2063. doi:10.1002/mrm.25746
Kaas JH. 2012. Somatosensory System. *The Human Nervous System*. doi:10.1016/b978-0-12-374236-0.10030-6

Kalisch T, Ragert P, Schwenkreis P, Dinse HR, Tegenthoff M. 2009. Impaired tactile acuity in old age is accompanied by enlarged hand representations in somatosensory cortex. *Cereb Cortex* **19**:1530–1538. doi:10.1093/cercor/bhn190

Kalisch T, Tegenthoff M, Dinse HR. 2008. Improvement of sensorimotor functions in old age by passive sensory stimulation. *Clin Interv Aging* **3**:673–690. doi:10.2147/cia.s3174

Kalisch T, Tegenthoff M, Dinse HR. 2007. Differential effects of synchronous and asynchronous multifinger coactivation on human tactile performance. *BMC Neurosci* **8**:58. doi:10.1186/1471-2202-8-58

Kang EY, Park Y, Li X, Segrè AV, Han B, Eskin E. 2016. ForestPMPlot: A Flexible Tool for Visualizing Heterogeneity Between Studies in Meta-analysis. *G3* **6**:1793–1798. doi:10.1534/g3.116.029439

Kelley DJ, Oakes TR, Greischar LL, Chung MK, Ollinger JM, Alexander AL, Shelton SE, Kalin NH, Davidson RJ. 2008. Automatic physiological waveform processing for FMRI noise correction and analysis. *PLoS One* **3**:e1751. doi:10.1371/journal.pone.0001751

Kikkert S, Kolasinski J, Jbabdi S, Tracey I, Beckmann CF, Johansen-Berg H, Makin TR. 2016. Revealing the neural fingerprints of a missing hand. *Elife* **5**. doi:10.7554/eLife.15292

Kikkert S, Mezue M, O'Shea J, Slater DH, Johansen-Berg H, Tracey I, Makin TR. 2019. Neural basis of induced phantom limb pain relief. *Annals of Neurology*. doi:10.1002/ana.25371

Kolasinski J, Makin TR, Jbabdi S, Clare S, Stagg CJ, Johansen-Berg H. 2016a. Investigating the Stability of Fine-Grain Digit Somatotopy in Individual Human Participants. *Journal of Neuroscience*. doi:10.1523/jneurosci.1742-15.2016

Kolasinski J, Makin TR, Logan JP, Jbabdi S, Clare S, Stagg CJ, Johansen-Berg H. 2016b. Perceptually relevant remapping of human somatotopy in 24 hours. *eLife*. doi:10.7554/elife.17280

Krüger G, Glover GH. 2001. Physiological noise in oxygenation-sensitive magnetic resonance imaging. *Magnetic Resonance in Medicine: An Official Journal of the International Society for Magnetic Resonance in Medicine* **46**:631–637.

Kuehn E, Dinse J, Jakobsen E, Long X, Schäfer A, Bazin P-L, Villringer A, Sereno MI, Margulies DS. 2017a. Body Topography Parcellates Human Sensory and Motor Cortex. *Cereb Cortex* **27**:3790–3805. doi:10.1093/cercor/bhx026

Kuehn E, Doehler J, Pleger B. 2017b. The influence of vision on tactile Hebbian learning. *Sci Rep* **7**:9069. doi:10.1038/s41598-017-09181-6

Kuehn E, Haggard P, Villringer A, Pleger B, Sereno MI. 2018. Visually-Driven Maps in Area 3b. *J Neurosci* **38**:1295–1310. doi:10.1523/JNEUROSCI.0491-17.2017

Kuehn E, Sereno MI. 2018. Modelling the Human Cortex in Three Dimensions. *Trends Cogn Sci* **22**:1073–1075. doi:10.1016/j.tics.2018.08.010

Lenz M, Tegenthoff M, Kohlhaas K, Stude P, Höffken O, Gatica Tossi MA, Kalisch T, Kowalewski R, Dinse HR. 2012. Increased excitability of somatosensory cortex in aged humans is associated with impaired tactile acuity. *J Neurosci* **32**:1811–1816. doi:10.1523/JNEUROSCI.2722-11.2012

Lix LM, Keselman JC, Keselman HJ. 1996. Consequences of Assumption Violations Revisited: A Quantitative Review of Alternatives to the One-Way Analysis of Variance "F" Test. *Rev Educ Res* **66**:579–619. doi:10.2307/1170654

Mair P, Wilcox R. 2020. Robust statistical methods in R using the WRS2 package. *Behav Res Methods* **52**:464–488. doi:10.3758/s13428-019-01246-w

Makin TR, Cramer AO, Scholz J, Hahamy A, Slater DH, Tracey I, Johansen-Berg H. 2013a. Deprivation-related and use-dependent plasticity go hand in hand. *eLife*. doi:10.7554/elife.01273

Makin TR, Scholz J, Filippini N, Henderson Slater D, Tracey I, Johansen-Berg H. 2013b. Phantom pain is associated with preserved structure and function in the former hand area. *Nat Commun* **4**:1570. doi:10.1038/ncomms2571

Mattay VS, Fera F, Tessitore A, Hariri AR, Das S, Callicott JH, Weinberger DR. 2002. Neurophysiological correlates of age-related changes in human motor function. *Neurology*. doi:10.1212/wnl.58.4.630

McGregor KM, Carpenter H, Kleim E, Sudhyadhom A, White KD, Butler AJ, Kleim J, Crosson B. 2012. Motor map reliability and aging: a TMS/fMRI study. *Exp Brain Res* **219**:97–106. doi:10.1007/s00221-012-3070-3

Miller TM, Schmidt TT, Blankenburg F, Pulvermüller F. 2018. Verbal labels facilitate tactile perception. *Cognition*. doi:10.1016/j.cognition.2017.10.010

O'Neill GC, Sengupta A, Asghar M, Barratt EL, Besle J, Schluppeck D, Francis ST, Sanchez Panchuelo RM. 2020. A probabilistic atlas of finger dominance in the primary somatosensory cortex. *Neuroimage* 116880. doi:10.1016/j.neuroimage.2020.116880

Overduin SA, d'Avella A, Carmena JM, Bizzi E. 2012. Microstimulation Activates a Handful of Muscle Synergies. *Neuron*. doi:10.1016/j.neuron.2012.10.018

Penfield W, Boldrey E. 1937. Somatic motor and sensory representation in the cerebral cortex of man as studied by electrical stimulation. *Brain* **60**:389–443.

Pilz K, Veit R, Braun C, Godde B. 2004. Effects of co-activation on cortical organization and discrimination performance. *Neuroreport* **15**:2669–2672. doi:10.1097/00001756-200412030-00023

Pleger B, Wilimzig C, Nicolas V, Kalisch T, Ragert P, Tegenthoff M, Dinse HR. 2016. A complementary role of intracortical inhibition in age-related tactile degradation and its remodelling in humans. *Sci Rep* **6**:27388. doi:10.1038/srep27388

Puckett AM, Bollmann S, Junday K, Barth M, Cunnington R. 2020. Bayesian population receptive field modeling in human somatosensory cortex. *Neuroimage* **208**:116465. doi:10.1016/j.neuroimage.2019.116465

R Core Team. 2019. R: A Language and Environment for Statistical Computing. R Foundation for Statistical Computing, Vienna, Austria.

Reiser MF, Semmler W, Hricak H. 2007. Magnetic Resonance Tomography. Springer Science & Business Media.

Reuter-Lorenz PA, Lustig C. 2005. Brain aging: reorganizing discoveries about the aging mind. *Curr Opin Neurobiol* **15**:245–251. doi:10.1016/j.conb.2005.03.016

Riecker A, Gröschel K, Ackermann H, Steinbrink C, Witte O, Kastrup A. 2006. Functional significance of age-related differences in motor activation patterns. *Neuroimage* **32**:1345–1354. doi:10.1016/j.neuroimage.2006.05.021

Robson MD, Gore JC, Constable RT. 1997. Measurement of the point spread function in MRI using constant time imaging. *Magn Reson Med* **38**:733–740. doi:10.1002/mrm.1910380509

Saadon-Grosman N, Tal Z, Itshayek E, Amedi A, Arzy S. 2015. Discontinuity of cortical gradients reflects sensory impairment. *Proceedings of the National Academy of Sciences*. doi:10.1073/pnas.1506214112

Schmidt TT, Blankenburg F. 2018. Brain regions that retain the spatial layout of tactile stimuli during working memory – A "tactospatial sketchpad"? *NeuroImage*. doi:10.1016/j.neuroimage.2018.05.076

Schweisfurth MA, Frahm J, Schweizer R. 2015. Individual left-hand and right-hand intra-digit representations in human primary somatosensory cortex. *European Journal of Neuroscience*. doi:10.1111/ejn.12978

Schweisfurth MA, Schweizer R, Frahm J. 2011. Functional MRI indicates consistent intra-digit

topographic maps in the little but not the index finger within the human primary somatosensory cortex. *Neuroimage* **56**:2138–2143. doi:10.1016/j.neuroimage.2011.03.038

Schweisfurth MA, Schweizer R, Treue S. 2014. Feature-based attentional modulation of orientation perception in somatosensation. *Front Hum Neurosci* **8**:519. doi:10.3389/fnhum.2014.00519

Schweizer R, Braun C, Fromm C, Wilms A, Birbaumer N. 2001. The distribution of mislocalizations across fingers demonstrates training-induced neuroplastic changes in somatosensory cortex. *Experimental Brain Research*. doi:10.1007/s002210100793

Schweizer R, Maier M, Braun C, Birbaumer N. 2000. Distribution of mislocalizations of tactile stimuli on the fingers of the human hand. *Somatosens Mot Res* **17**:309–316. doi:10.1080/08990220020002006

Schweizer R, Voit D, Frahm J. 2008. Finger representations in human primary somatosensory cortex as revealed by high-resolution functional MRI of tactile stimulation. *Neuroimage* **42**:28–35. doi:10.1016/j.neuroimage.2008.04.184

Sereno MI, Huang R-S. 2006. A human parietal face area contains aligned head-centered visual and tactile maps. *Nat Neurosci* **9**:1337–1343. doi:10.1038/nn1777

Smith SM, Jenkinson M, Woolrich MW, Beckmann CF, Behrens TEJ, Johansen-Berg H, Bannister PR, De Luca M, Drobnjak I, Flitney DE, Niazy RK, Saunders J, Vickers J, Zhang Y, De Stefano N, Brady JM, Matthews PM. 2004. Advances in functional and structural MR image analysis and implementation as FSL. *Neuroimage* **23 Suppl 1**:S208–19. doi:10.1016/j.neuroimage.2004.07.051

Sokal RR, Rohlf FJ. 1981. Biometry WH Freeman. *New York* 859.

Spengler F, Godde B, Dinse HR. 1995. Effects of ageing on topographic organization of somatosensory cortex. *Neuroreport* **6**:469–473. doi:10.1097/00001756-199502000-00016

Stanislaw H, Todorov N. 1999. Calculation of signal detection theory measures. *Behav Res Methods Instrum Comput* **31**:137–149. doi:10.3758/bf03207704

Stringer EA, Qiao P-G, Friedman RM, Holroyd L, Newton AT, Gore JC, Min Chen L. 2014. Distinct fine-scale fMRI activation patterns of contra- and ipsilateral somatosensory areas 3b and 1 in humans. *Hum Brain Mapp* **35**:4841–4857. doi:10.1002/hbm.22517

Timm F, Kuehn E. 2020. A Mechanical Stimulation Glove to Induce Hebbian Plasticity at the Fingertip. *Front Hum Neurosci* **14**:177. doi:10.3389/fnhum.2020.00177

Van Beek N, Stegeman DF, Jonkers I, de Korte CL, Veeger D, Maas H. 2019. Single finger movements in the aging hand: changes in finger independence, muscle activation patterns and tendon displacement in older adults. *Exp Brain Res* **237**:1141–1154. doi:10.1007/s00221-019-05487-1

Woolrich MW, Jbabdi S, Patenaude B, Chappell M, Makni S, Behrens T, Beckmann C, Jenkinson M, Smith SM. 2009. Bayesian analysis of neuroimaging data in FSL. *Neuroimage* **45**:S173–86. doi:10.1016/j.neuroimage.2008.10.055

Wu M, Kumar A, Yang S. 2016. Development and aging of superficial white matter myelin from young adulthood to old age: Mapping by vertex-based surface statistics (VBSS). *Hum Brain Mapp* **37**:1759–1769. doi:10.1002/hbm.23134

Zeharia N, Hertz U, Flash T, Amedi A. 2015. New whole-body sensory-motor gradients revealed using phase-locked analysis and verified using multivoxel pattern analysis and functional connectivity. *J Neurosci* **35**:2845–2859. doi:10.1523/JNEUROSCI.4246-14.2015

Zeharia N, Hofstetter S, Flash T, Amedi A. 2019. A Whole-Body Sensory-Motor Gradient is Revealed in the Medial Wall of the Parietal Lobe. *J Neurosci* **39**:7882–7892. doi:10.1523/JNEUROSCI.0727-18.2019

Zeidman P, Silson EH, Schwarzkopf DS, Baker CI, Penny W. 2018. Bayesian population

receptive field modelling. *Neuroimage* **180**:173–187. doi:10.1016/j.neuroimage.2017.09.008